*Revision with No Changes Marked
Click here to view linked References

The dolomite nodules enclosing fossil marine vertebrates in the East Pisco Basin, Peru: field and petrographic insights into the Lagerstätte formation

Karen Gariboldi[ab], Anna Gioncada[a], Giulia Bosio[c], Elisa Malinverno[c], Claudio Di Celma[d], Chiara Tinelli[a], Gino Cantalamessa[d], Walter Landini[a], Mario Urbina[e] and Giovanni Bianucci[a]

[a]Dipartimento di Scienze della Terra, Università di Pisa, via Santa Maria 53, 56126, Pisa, Italy

[b]Dottorato Regionale Toscano di Scienze della Terra Dipartimento di Scienze della Terra, Università di Pisa, via Santa Maria 53, 56126, Pisa, Italy

[c]Dipartimento di Scienze dell'Ambiente e del Territorio e di Scienze della Terra (DISAT) Sezione di Scienze Geologiche e Geotecnologie, Università degli Studi di Milano-Bicocca, Piazza della Scienza, 4
20126 Milano, Italy

[d]Scuola di Scienze e Tecnologie, Università di Camerino, Piazza dei Costanti 4, 62032, Camerino, Macerata, Italy

[e]Departamento de Paleontologia de Vertebrados, Museo de Historia Natural-UNMSM, Avenida Arenales 1256, Jesús María, Lima 14, Peru

Corresponding author: Karen Gariboldi Email: karen.gariboldi@for.unipi.it

Abstract

The Mio-Pliocene Pisco Formation (Peru) is a worldwide famous marine vertebrate Lagerstätte. Several fossil specimens are wrapped up in dolomitic nodules. Some others lie in the sediment displaying dolomite only in bone cavities (e.g., mesorostral canal and endocranium). With the aim to understand whether the precipitation of the dolomitic nodules influenced the formation of the Lagerstätte, we collected field data on a high number of fossil vertebrates and conducted petrographic and mineralogical analyses on samples representative of the variable development of concretions. Our results revealed positive relationships between size, completeness and articulation of skeletons and the presence of an external nodule. Clear evidence of chemoautotrophic communities that thrived on the carcasses are scarce. Microborings are often found in the cortical bone tissues together with iron oxides; the former are left by microorganisms feeding on the carcass, the latter are traces of former Fe sulphides, a product of organic matter degradation. We suggest that an early burial of the skeletons was a determinant factor in the development of dolomite concretions, since it allowed methanogenesis and anaerobic sulphate reduction exploiting the lipids in the bones and the organic matter dispersed in the sediments. Dolomite precipitation was driven by the same bacteria operating during the suphophilic stage of whale-fall communities. Textural observations imply that dolomite precipitated shortly after carcasses burial. The increase of alkalinity generated by sulphate reduction and methanogenesis caused rapid precipitation of dolomite within skeletal cavities and prevented the degradation of the bones and diagenetic compression of skeletons; nodules themselves prevented erosion of fossils after exhumation. Therefore, nodules formation had a crucial role in the development of the Pisco Lagerstätte**.**

Keywords: biomineralization, dolomite concretions, marine vertebrates, taphonomy, Pisco Formation.

1. Introduction

The Mio-Pliocene, mainly diatomaceous, Pisco Formation, crops out in the Ica desert, Peru. For decades, due to its enormous concentration of perfectly preserved fossil marine vertebrates (Esperante et al., 2008), it has been raising the interest of researchers from all over the world. This interest has been raised by the

49 opportunity to study in detail the evolution of many vertebrates lineages (e.g., Bianucci et al., 2010; Lambert
50 et al., 2008, 2009, 2010, 2013 and references therein) and taphonomy (Ehret et al 2008, Esperante et al.,
51 2008, 2015). Due to fossil abundance and preservation, the Pisco Fm. can be defined as a Konservat-
52 Lagerstätte (Seilacher, 1970; Esperante et. al., 2015).

53 The fossil vertebrates of the Pisco Fm., are often enclosed in hard dolomite concretions, or nodules. Even
54 in absence of the carbonate concretion, sediments close to the fossil bones are commonly lithified and have a
55 different colour in respect to the surrounding lithology.

56 Carbonate concretions enclosing fossils have been described from the Pisco Fm. (Esperante et al., 2015)
57 as well as from many other deposits (e.g.,Tarr, 1921; Weeks, 1957; Canfield and Raiswell, 1991; Kaim et al.,
58 2008; Danise et al., 2012; McCoy, 2015 and references therein). Hypotheses on their relation with the decay
59 processes have been proposed for both invertebrates and vertebrates (e.g., Briggs, 2003; Danise et al., 2012).
60 Information on the paleo-geochemical micro-environments related to the pre-burial decay and early
61 diagenesis of fossil marine vertebrates has been gained by observations on modern shallow- and deep-water
62 whale fall communities (Allison et al., 1991; Goffredi et al., 2004; Treude et al., 2009; Little, 2010). This
63 subject is still matter of discussion, in particular as regards: 1) the development of a sulphophilic stage
64 supporting chemoautotrophic communities on shallow fossil whale falls (Dominici et al., 2009; Danise et al.,
65 2012, 2014); 2) the early vs. late diagenetic origin for carbonate cements precipitated within the skeletons
66 (Kiel, 2008; Shapiro and Spangler, 2009). However, most of the studies on this topic still focus on a limited
67 number of specimens and lack a basin-scale field background.

68 The abundance of concretions enclosing fossil vertebrates in the Pisco Fm. and their variable
69 development and characteristics give the opportunity to study the formation mechanisms of concretions; the
70 aim is to provide results for future reconstructions of the fossilization processes. We suggest that the
71 dolomite concretions hosting fossil vertebrates can give important insights into: 1) the geochemical processes
72 occurring during and as a consequence of decay; 2) the interaction between the decaying carcass and the
73 enclosing sediment. Relation between high sedimentation rates and the formation of the Pisco Konservat-
74 Lagerstätte formation have been proposed by Esperante et al. (2008); however, we believe that many are the
75 causes that contributed to the Lagerstätte. In this frame, our research aims (i) to carry out a reconstruction of

76 nodule formation mechanisms, (ii) to assess their temporal relationships with the fossilization process and
77 (iii) to evaluate their role in the fossil preservation, basing our investigations on the large variety of records
78 offered by the Ica desert Konservat-Lagerstätte. With these purposes, in this work we discuss the results
79 driven from field investigations, providing a complete picture of the variable development of concretions
80 around the fossil. We also discuss the results of petrographic and mineralogical investigations conducted on
81 selected representative specimens.
82
83 **2. Geological frame**
84
85 The Pisco Formation crops out for about 300 km along the southwestern coast of Peru, from Pisco to
86 Yauca (Fig. 1A, B), its thickness ranging from about 200 to 1000 m (Dunbar et al., 1990). The Formation
87 was deposited during the Mio-Pliocene in the East Pisco forearc basin (Thornburg and Kulm, 1981; De
88 Muizon and DeVries, 1985; DeVries, 1988) and subsequently uplifted starting from the late Pliocene, most
89 of the uplift being caused by the subduction of the aseismic Nazca ridge under the South American Plate
90 (Hsu, 1992). Communications of the basin with the outer ocean were restricted due to two structural barriers:
91 the Mesozoic igneous rocks of the Coastal Batholith to the east (Mukasa, 1986; Cobbing, 1999) and by
92 Precambrian and Jurassic metamorphic, igneous and sedimentary rocks of the Coastal Cordillera to the west
93 (Romero et al., 2013). Nowadays, the East Pisco Basin belongs to a morphostructural unit known as
94 “Pampas Costera” (Coastal Desert), a desert region cluttered with numerous hills with a large base and a
95 planar top, modeled during Quaternary by marine and continental erosion phenomena (Montoya et al., 1994).
96 Our study area, the Ica Desert, is characterized by these morphologies (Fig. 1C).
97 Because of the coastal upwelling conditions characterizing the Peruvian shelf since the Miocene (Suess
98 and von Huene, 1988), the East Pisco Basin was characterized by continuous diatom blooms causing a high-
99 rate biosiliceus sedimentation. Therefore, diatomaceous mudstones are the main lithology characterizing the
100 Pisco Fm., in particular in its upper portion (Brand et al., 2011). Nodular dolomite layers, terrigenous
101 sandstones, tuff beds from the Andean volcanic activity and minor phosphorites complete the sequence
102 (Dunbar et al., 1990; Brand et al., 2011; Di Celma et al., 2015).

103 This work is mainly focused on the outcrops of Cerro Colorado (late Miocene; Di Celma et al., 2015) and
104 Cerro Los Quesos (late Miocene; Brand et al., 2011; Di Celma et al., submitted) (Fig. 1B).
105
106 **3. Methods**
107 Field surveys were conducted in July 2013, May 2014 and September 2014 at Cerro Colorado and Cerro
108 Los Quesos. Stratigraphic investigations were carried out together with acquisition of paleontological data
109 and collection of samples for petrographic and micropaleontological analyses.
110 A total of 229 fossil vertebrates (preserved as bone elements), out of those recorded in field surveys were
111 used for this study (156 specimens at Cerro Colorado and 73 at Cerro Los Quesos).
112 For each fossil, detailed information was reported in dedicated sheets filled-out in the field. These data
113 consist of: 1) the location (carefully recorded using hand-held GPS devices); 2) a preliminary identification
114 (see Bianucci et al., 2015 for Cerro Colorado); 3) the stratigraphic position; 4) several accurate taphonomic
115 observations (e.g., skeleton completeness, defined as percentage of skeleton preserved and articulation,
116 defined as percentage of skeletal elements still articulated -see Tables S1 and S2, supplementary material-;
117 evidences scavengers (e.g. shark bites); presence of mollusks and/or shark teeth associated to the carcasses);
118 5) observations on the enclosing sediments (e.g., color and degree of lithification and development of the
119 concretions).
120 For the petrographic and mineralogical analyses, we collected samples of bones, nodules and sediments
121 enclosing the bones and nodules,with the aim of analyzing all the cases of nodules development. A synthetic
122 description is reported in Table 1. Samples were selected for laboratory analyses. We also collected samples
123 of unlithified diatomite surrounding the nodules and of dolomitic stratigraphic layers, which formed
124 morphological benches along the sequence.
125 The samples were examined under a stereoscope. Polished thin sections of bones and enclosing
126 sediments were observed by means of a petrographic microscope Axioplan in transmitted and reflected light.
127 Scanning Electron Microscopy in Backscattered Electron Imaging (SEM-BSEI), Secondary Electron
128 Imaging (SEM-SEI) and Energy Dispersive X-Ray Spectroscopy analyses (EDS) of sediment particles,
129 cement, bones and pore filling minerals were carried out with a Philips XL30 equipped with a Dx4i

130 microanalytical device on the same carbon-coated polished thin sections at Dipartimento di Scienze della
131 Terra of the University of Pisa (Italy). Analytical details were 20 kV filament voltage, 5 nA beam current,
132 100 s counting time, ZAF correction. Major elements composition of the bulk nodule was estimated through
133 EDS analysis of scanned windows of 1 mm x 1 mm and 500 µm x 500 µm, selected to have a sufficiently
134 large area compared to the sediment grain size; rare and scattered particles larger than 250 micron were
135 avoided from the analyses. Fragments of lithified sediment were picked up and carbon-coated to be observed
136 by means of SEM as well. X-ray Powder Diffraction (XRPD) analyses were carried out with a Philips
137 diffractometer at Dipartimento di Scienze della Terra of Pisa on bulk sediment samples, after pulverization in
138 an agate mortar.
139
140 **4. Results**
141
142 *4.1. Field data*
143 The sedimentological structures observed in the field suggest that the depth of the Pisco Basin at both
144 Cerro Colorado and Cerro Los Quesos ranged between 0 and 100 m bsl (inner-middle shelf). Cerro Colorado
145 is characterized by evidences of a strong terrigenous input, while biosiliceous sediments prevail at Cerro Los
146 Quesos. Nodules enclosing fossils are present in all the lithologies characterizing the investigated sites:
147 laminated diatomite, diatomaceous silt and fine sand. These nodules are rounded, roughly cylindrical
148 concretions, with variable size, depending on the size of the fossil (more than 10 m for some mysticetes of
149 Cerro Los Quesos). Due to the greater resistance of dolomite to erosion compared to the surrounding
150 lithologies, these features are easily recognizable at the outcrop (Fig. 1C). The concretions are in contact
151 with the cortical part of the fossil bones and can be over 10 cm thick, thus hiding the presence of the
152 skeletons to an inexperienced observer (Fig. 1C; Fig. 2A, B, C). On the other hand, several fossil vertebrates
153 emerge from the ground without being wrapped in an external nodule (Fig. 3 A, B). Nonetheless, in most
154 cases, these display carbonate concretions within the trabecular tissue of bones, in cavities within bones (e.g.,
155 endocranium, mesorostral canal, neural arc of vertebrae) or between adjacent articulated bones (e.g.,
156 vertebrae), indicating a partial development of nodule (Fig. 2D, E). The bones interested by dolomite

concretions filling bone cavities do not display diagenetic compression features. In some cases, deformation of the underlying sediment shows clear evidence that the carcasses at least partially sank into the seafloor. Overall, the sediment interested by the dolomitic concretions is massive and bluish-ocre to yellow-ocre in color. Below the concretions, a particular sequence of colors grading to the undisturbed surrounding sediment has been repeatedly recognized: right below the concretions the sediment is non-laminated, yellow and then reddish in color, with a millimeter-thick black band separating the yellow from the reddish zone. This sequence of yellow-black-red sediments (YBR sequence hereafter) is some centimeters to a few decimeters thick. Because the sediment overlying nodules is only partially preserved, clear indications on the presence of the complete YBR sequence above the nodules cannot be given. The YBR sequence has been observed also in absence of the dolomite nodules, the yellow sediment being directly in contact with the bones (Fig. 3A, B). Some specimens neither have dolomite, neither display a visible YBR sequence (Fig. 3C).

At Cerro Los Quesos, only eight specimens out of the 73 examined (11%) present dolomitic concretions. At Cerro Colorado, the presence of dolomite is much more frequent, interesting 68 of the 157 examined specimens (44%, Fig. 4A, B). The elevated number of fossils with dolomitic concretions at Cerro Colorado allowed us 1) to check for relations between the presence of nodules and some taxonomic and taphonomic features of the specimens, such as the taxon they belong to, their size, skeletal articulation and completeness (Fig. 4C, D, E); 2) to evaluate their vertical and horizontal distribution in the stratigraphical sequence (Fig. 4A).

The Cerro Colorado fossil vertebrates mostly belong to cetaceans, representing 86% of the specimens examined for the presence of concretions. Cetaceans that were identified are mysticetes (cetotheriids and balaenopteroids) and odontocetes (kentriodontid-like delphinidans, pontoporiids, ziphiids and physeteroids including the giant raptorial sperm whale *Livyatan melvillei*, Lambert et al., 2010). Besides cetaceans, seals, crocodiles, sea turtles, seabirds, bony fish, and sharks are reported (Bianucci et al., 2015).

The nodules mainly occur in correspondence of cetacean remains, and are definitely more frequent in mysticetes (67% of remains present a high or partial development of concretions) than in odontocetes (22% of remains) and in pinnipeds (14%) (Fig. 4C). The higher frequency of nodules in the cetaceans in respect to

184 other vertebrates and, within the cetaceans, in the mysticetes rather than the odontocetes, evidences a
185 relationship between the fossil size and the presence or absence of nodule. In fact, at Cerro Colorado the
186 skeletons of mysticetes are generally larger than the ones of odontocetes and, on the whole, the cetacean
187 skeletons are in most cases larger than the ones of other marine vertebrates. A relationship also exists
188 between the presence of a nodule and both the articulation (Fig. 4D) and the completeness (Fig. 4E) of the
189 fossil skeletons, i.e. the specimens with a highly or partially developed nodule are preferentially totally or
190 partially articulated and complete.

191 The distribution of the fossil vertebrates inspected for concretions at Cerro Colorado along the
192 stratigraphic column is illustrated in Fig. 4A. Nodules are not concentrated in a particular stratigraphic
193 position, instead they affect specimens irrespective of their stratigraphic position, suggesting that the nodule
194 formation is not related to a given sedimentary event.

195 Shark teeth have been found associated to fossils, but evident traces of shark bites on bones are rare; any
196 other evidence of scavenging activity (e.g., crustaceans) is absent. On the other hand, both at Cerro Colorado
197 and at Cerro Los Quesos bivalves are present, being frequent but unrelated to fossil vertebrates at Cerro
198 Colorado and rare butassociated to fossil cetaceans at Cerro Los Quesos. Bivalves from Cerro Colorado
199 mostly belong to the genera *Dosinia* and *Anadara* (suspension feeders), while bad preservation of specimens
200 prevented the determination of bivalves from Cerros Los Quesos. Bivalves at Cerro Los Quesos are still in
201 their living position.

202

203 *4.2 Petrography and mineralogy*

204

205 The specimens selected for the petrographic and mineralogical studies of the concretions (Table 1) are
206 representative of the different situations encountered in the field. We summarized the diverse situations
207 encountered into three cases: 1) specimens enclosed in a hard dolomitic nodule; 2) specimens with partially
208 developed dolomite concretions (mainly within cranium and rostrum cavities, between two articulated
209 vertebral bodies and in the neural arch of vertebrae); 3) specimens without dolomitic nodule, hosted in a
210 partially hardened sediment of yellow-reddish color. Sampling strategy is shown in Fig. 5A. We sampled

211 both the nodules and the bones, at different skeletal positions, when available. Oriented subsamples were
212 selected to study the nodule development at the microscopic scale (Fig. 5B).
213
214 *4.2.1. The dolomite nodules enclosing fossil bones*
215 The petrographic study highlighted that concretions consist of variable fractions of diatomaceous or
216 terrigenous clasts, of microcrystalline carbonate and of void-filling sparry carbonate cements (Fig. 6A). Both
217 the microcrystalline and the sparry carbonate are dolomite. The micritic dolomite shows a clotted texture.
218 The sediment clasts consist of diatom frustules joined to terrigenous mineral grains, volcanic ashes and
219 forams in variable amounts (Fig. 6A, B, C, D). In the most consolidated concretions, SEM imaging
220 highlights that dolomite completely fills not only the intergranular porosity, but also the small areolae of
221 diatom valves (Fig. 6B). In some cases, silica of diatom valves is dissolved and the morphology of diatoms is
222 perfectly replicated by molds of dolomite. Foraminifera tests can be replaced by dolomite.
223 The dolomite cement fills completely the original sediment porosity close to the bones as well as most
224 bone cavities (Fig. 5B), while the porosity is progressively left unfilled moving out of them (Fig. 5C). At the
225 outcrop scale, the more cemented regions correspond to a light bluish carbonate rock, while the porous
226 regions have a yellow/reddish color.
227 The dolomite cement has a crystal size of about 50 microns and displays a mosaic texture when filling
228 diatom frustules or foram tests. Compared to the diatomaceous mudstone out of the nodules at a similar
229 stratigraphic position, diatom frustules preserved within the nodules are overall scarcely deformed (Fig. 7).
230 In most cases, the dolomite-cemented diatomaceous sediment is massive (Fig. S1A, supplementary
231 material). Only two examples of concretions preserving the laminated pattern of the original sediment were
232 found: these are the external nodule of specimen CC-O46 (Fig. S1B, supplementary material) and the
233 mesorostral canal nodule of specimen CLQ-M67 (Table 1). In both cases the laminae are millimeter or
234 submillimeter in thickness and are alternately dominated by biogenic and terrigenous particles. The
235 terrigenous laminae of specimen CC-O46 are characterized by terrigenous particles of ca. 100 μm of
236 diameter cemented together by dolomite, while the diatom genus *Actinoptychus* seems to dominate the
237 biogenic fraction. On the other hand, specimen CLQ-M67 seems to be dominated by biogenic laminae

238 (frustules of the diatom genus *Coscinodiscus* are easily recognizable), while the terrigenous fraction is
239 represented by an aphanotopic cement probably binding together fine clay particles. An estimation of the
240 chemical composition of the nodules has been obtained by averaging several EDS scans of 1 mm x 1 mm
241 500 µm x 500 µm areas (Table 2). Major elements chemical composition at increasing distances from the
242 bones indicates a decrease of Ca and Mg in respect to Si, and an increase of the Al/Si ratio (Table 2): these
243 trends confirm the increase of dolomite filling towards the bones, as visible in SEM-BSE images (Fig. 5C).
244 Fine-grained iron oxides/hydroxides (from <0.5 µm to ca. 2.5 µm, in clusters of 10 µm in diameter) are
245 rather diffuse in the dolomite-cemented sediment, in particular inside diatom frustules and around them. The
246 prevalent shape and clustering of fine rounded grains (Fig. 6C) is suggestive of replacement of previous iron
247 sulphide framboids: indeed, iron sulphides can be altered to iron oxides in oxic condition (Eggleston et al,
248 1996).
249 Within bones, dolomite fills cavities such as Haversian canals and trabecular porosities (Fig. 5B) with
250 different textures: fine anhedral crystals, clotted aggregates, mosaic shaped crystals, bladed or mosaic-shaped
251 void-fillings. Terrigenous and biosiliceous clasts also entered some bone cavities. The bone tissues enclosed
252 in dolomite concretions do not show any mineral replacement and structures such as Haversian canals are
253 preserved. In some cases the trabecular tissue can be fractured (Fig. 6D) and the cortical tissue intensely
254 burrowed (Fig. 8A, B, C). We recognized at least three types of borings. Microborings type A are 2-4 µm in
255 diameter and around 30-40 µm in length (Fig. 8A) although their size and shape are comparable to those of
256 microborings type 1 described by Danise et al. (2012), they differ from the latter by interesting only the
257 cortical tissue and not the trabecular one. Iron oxides have been observed in correspondence of microborings
258 type 1 (Fig. 8A, arrows). Danise et al., 2012 identified those as traces left by some kind of organisms of
259 prokaryotic origin. Microborings type B have lengths ranging between 10 and 20 µm and diameters of ca.
260 12,5 µm (Fig. 8B). These microborings are limited to the first 50 µm of the cortical bone tissue (Fig. 8B).
261 Although we are not able to identify the organism which left these traces, they seem to be the same
262 represented in Fig.13D of Esperante et al. (2015), described as Wedl type tunnels; however, the length and
263 the diameter of microborings type B do not fit the description of Wedl type tunnels, which are described as
264 tunnels of 8 µm of diameter penetrating for 0.2-0.25 mm below the bones surface (Davis, 1997).

Microborings type C are found on the cortical tissue; they are tubular and have lobe-like extensions, with diameters of ca. 35 μm and length of ca. 100-120 μm (Fig. 8C); their shapes resemble traces left by *Osedax* spp. (Kiel et al., 2010, 2013; Higgs et al., 2014), but they are too small to be unambiguously attributed to this organism. The textural relationships between the mineral phases infilling pore spaces in bones within nodules indicate that dolomite was the first mineral to grow as an infill, nucleating on the bone surface. At the contact with the bone, the sediment particles may be separated from the cortical bone by a thin dolomite rim, apparently exploiting the bone as a nucleation surface and in some cases showing a clotted textures (Fig. 6E). The cloudy reddish opaques visible in transmitted light (Fig. 6A, D) (corresponding to the bright punctuations under SEM-BSE, Fig. 6F, arroheads) indicate that iron oxides precipitated, probably as sulphides, during dolomite growth. In the cavities of trabecular bone which were not invaded by sediment, a second generation of dolomite cement grew nucleating on the first generation dolomite originating a drusy texture. An evident zoning in Fe content in the drusy dolomite is revealed by SEM-BSEI images and EDS microanalytical data (Fig. 6G and Table 2). A final dolomite cement fills the drusae as sparry mosaic dolomite. Silica, also, is found as cement. Textural relationships in correspondence of small cracks with negligible displacement in the trabecular bone (Fig. 6D) highlight the continuity of the dolomite-cemented sediment and of the dolomite rimming the bone along the fractured surface. This pattern indicates that many cracks occurred before the first generation of dolomite and shortly before nodule consolidation.

Late minerals (gypsum, anhydrite, halite, Mn minerals) are found in the bones and are also diffusely present in the nodules, with textural relationships indicating that they formed after the carbonate cement. Part or all gypsum/anhydrite occurs filling poresand drusae and as diffuse needles in intergranular positionand as veinlets; gypsum and anhydrite can be related to the several generations of gypsum veins of some centimeters of thickness, with fibrous texture, well evident in the field at both Cerro los Quesos and Cerro Colorado sites. Mn minerals (oxides) occur in the nodules as spots and veinlets or as patinae on the bones, suggesting that they formed after the carbonate cement (Fig. S2 supplementary material).

The dolomite layers forming discrete strata along the stratigraphic sequences are petrographically similar to the nodules enclosing fossil vertebrates as regards the texture of the carbonate. Here fish scales are rather common.

292

293 *4.2.2. The outer boundaries of the nodules: the YBR sequence*

294 Sediments from the different layers of YBR sequences have been investigated both by means of SEM-
295 EDS and XRPD analyses. These sediments are always scarcely lithified. The presence of ferroan dolomite is
296 highlighted in the yellow sediments (specimens CC-M85 and CLQ-M58, XRPD analysis) and minor
297 dolomite was found in specimen CLQ-C67 (SEM-EDS).

298 The black layer is composed mainly by Mn minerals, cementing the original sediment particles, while the
299 red layer presents dispersed Fe hydroxides. XRPD analyses carried out on the black layer did not permit the
300 identification of the Mn minerals due to low crystallinity.

301 Silica of the diatom frustules has been recognized both in the yellow and in the red layer, while it is
302 dissolved within the black layer and the original presence of diatoms is testified by their Mn-internal mould
303 (Fig. 6H).

304

305 **5. Discussion**

306

307 Dolomite layers are commonly observed in recent and past organic carbon-rich marine sediments (e.g.
308 Kulm et al., 1984; Benoulli and Gunzenhauser, 2001; Meister et al., 2008). Their formation has been related
309 to degradation of organic matter by different mechanisms: 1) anaerobic oxidation of methane (AOM), 2)
310 methanogenesis (MG) and 3) sulphate bacterial reduction (SBR). These mechanisms regulate carbonates
311 precipitations by increasing alkalinity and pH in sediment pore waters (Irwin et al., 1977; Jørgensen, 1992;
312 Coleman, 1993; Teal et al. 2000; Aloisi et al., 2002; Luff and Wallmann, 2003; Moore et al., 2004; Meister
313 et al., 2007, 2011, 2013). The inhibiting effect of sulphate on dolomite precipitation can be neutralized by
314 high sedimentation rates limiting sulphate penetration in the sediment (Kelts and Mackenzie, 1984) or by the
315 biomediated sulphate reduction operated by bacteria during organic matter degradation. The role of
316 biomediated sulphate reduction in dolomite formation has been also demonstrated by several laboratory
317 experiments (Vasconcelos et al., 1995; Van Lith et al., 2003; Jinhua et al., 2013; Bontognali et al., 2014).

318 Previous experimental results have explained the mechanisms for the formation of carbonate nodules
319 around decaying organisms (Berner, 1968; Allison, 1988): carbonate species may form in the environment
320 of decomposing carcasses following the increasing of alkalinity accompanied by a rise in pH (e.g. caused by
321 ammonia production); subsequently these may function as nucleation centers for binding additional
322 bicarbonate scavenged from pore-water (Allison, 1988). Geochemical studies of carbonate concretions in
323 marine environments confirm the role of organic matter decay processes (AOM, SBR, methanogenesis) in
324 their early diagenetic formation (Claypool and Kaplan, 1974; Irwin et al., 1977; Coleman, 1993, Bojanowski
325 and Clarkson, 2012). Recently, it has been suggested that nodules on large carcasses of vertebrates could be
326 linked to the activity of sulphate reducing bacteria (Shapiro and Spangler, 2009), and a correlation with the
327 evolution of modern whale-falls communities has been hypothesized (e.g., Danise et al., 2012). However,
328 additional observations on fossil vertebrates are needed to contribute to this discussion and to highlight the
329 role played by carbonate concretions in the formation of the Lagerstätte.
330
331 *5.1 Causes and timing of dolomite nodules formation*
332
333 The data collected during our field investigations in the Pisco Lagerstätte highlight that an important
334 relationship exists between fossil vertebrates and the presence of dolomite concretions (Fig. 2). Large,
335 complete and articulated fossils are characterized by concretions more frequently than the others (Fig. 4B, C,
336 D, E).
337 In the examined nodules, dolomite cements the intergranular and intragranular porosity of the preexisting
338 sediment, after it infilled the skeletal cavities (e.g., mesorostral canal, endocranium, neural arch of
339 vertebrae). Therefore, dolomite formation must have occurred after the whale soft tissues were already
340 decayed or taken away from the bones, and the bones themselves were, at least partially, covered by
341 sediment (Fig. 9A, B). Rapid burial may have been favoured by the sinking of the carcasses into the
342 unconsolidated sediment, as also suggested by Brand et al. (2004). Extremely high sedimentation rates have
343 been hypothesized for the Pisco Fm. (Brand et al., 2004; Esperante et al., 2015), but have not been measured
344 yet.

345 The infilling of trabecular bone and skull cavities by sediment can be explained as the result of suck in
346 due to the lower internal pressure caused by escaping of gases produced during organic matter degradation,
347 as proposed by Bodzioch and Kowal-Linka (2012). Thus, the infilling of the carcasses by the unconsolidated
348 sediments must have occurred shortly after or during degradation of soft organic matter in the cavities of the
349 skeleton, at the sea bottom or a few centimetres below it.

350 A subtle layer of dolomite crystals grown on the trabeculae surface and separating it from the sediment
351 clasts (Fig. 6E) testifies the early precipitation of at least the first generation of dolomite cement, nucleating
352 on the bones before the sediment completely filled the voids of the trabecular tissue.

353 The formation of dolomite inside the skeletal and bone cavities prevented the failure of the bones due to
354 the sedimentary load, which is instead observed in other cases in absence of carbonate nodules (e.g., the skull
355 of the holotype of *Nazcacetus urbinai* Lambert et al., 2009 from Cerro Los Quesos lacks endocranial
356 dolomitic concretion and presents a strong dorsolateral compression). Similarly, the scarce deformation of
357 diatom frustules in the nodules, compared to the diatomite out of the nodules, suggests that dolomite
358 precipitation mostly occurred before complete compaction (Fig. 7). On the other hand, the mosaic-textured
359 carbonate cement filling frustules, as well as the sparry cements in the trabecular porosity, represent one or
360 more later generations of dolomite cement precipitation, whose timing in respect to the formation of the main
361 concretions is difficult to assess; however, it precedes the precipitation of late minerals such as halite and
362 gypsum. Taken as a whole, the above evidences indicate that the dolomite nodules formed in several steps,
363 due to early diagenetic processes, after the sediment covered the bones (Fig. 9B), while a later step of sparry
364 dolomite filling is temporally unconstrained.

365 As regards the mechanism of dolomite formation, we favour primary dolomite precipitation as a main
366 mechanism, over secondary dolomitization. We found no clear petrographic evidence of dolomitization of a
367 previous calcite cement. Moreover, the petrographic features indicate the presence of clotted dolomite
368 textures and a close relationships between dolomite and iron oxides within the nodules. Framboids of iron
369 oxides, formerly sulphides, are recurrent; in addition, iron oxide inclusions occur in dolomite growing on the
370 bone trabeculae (Fig. 6F). Both clotted textures, associated iron oxides, and iron oxides in microborings can
371 be taken as evidence of microbial-mediated origin for the carbonate. Clotted textures can be consequent to

372 micro-geochemical variations related to bacterial activities (Kennard and James, 1986; Burne and Moore,
373 1987; Riding, 2000). For what concerns iron oxides H_2S is an intermediate product of decay processes and
374 its reaction with Fe takes to the production of iron mono-sulphides, later converted to pyrite in sulphidic
375 conditions and that we observed in the form of iron oxides (Fig. 6C, D, F, 8A). Although pyrite may be the
376 results of different reactions (Berner 1980, 1984), pyrite in the peripheral areas of bones and associated to
377 microborings is closely related to anaerobic sulfate reduction acting during lipids degradation (Shapiro et
378 Spangler, 2009; Danise et al., 2012). Indeed, these areas match with sulfide concentrations during lipid
379 degradation in modern whale–falls (Allison et al., 1991; Deming et al., 1997). Allison et al. (1991) also
380 suggest extensive skeletonisation (removal of soft tissue from carcasses) as a prerequisite for sulfide
381 formation in bones, as only this condition would permit oxygen and sulfate diffusion in the trabeculae.
382 For what the drusy dolomite in trabecular cavities is concerned, SEM-EDS analyses highlighted zoned
383 crystals with increasing Fe in the dolomite lattice (Fig. 6G) rather than with iron oxides. This indicates the
384 establishment of reduced but non-sulphidic conditions inside the drusae. Precipitation of the drusy dolomite
385 may be representative of a locally different geochemical microenvironment or of a later diagenetic stage
386 compared to that characterized by the presence of framboids. It can be assumed that microsparitic to sparry
387 dolomite infilling took place when no organic matter was left, as suggested in Riding and Tomás' model
388 (2006).
389 The microbially mediated precipitation of dolomite is supported by the massive texture (loss of
390 laminations) of nodules. This may be caused by an intense microbioirrigation activity (Pike et al., 2001) but
391 possibly also by the generation of methane, that typically gives a foamy appearance to the sediment (Treude
392 et al., 2009). Indeed, the laminations sporadically preserved in the external nodule of specimen CC-O46 and
393 the intrarostrum nodule of specimen CLQ-M67 testify that the loss of the original sedimentary features in
394 nodules was not induced by dolomite precipitation itself.
395 As regards the different microbially mediated processes involved in organic matter decay in marine
396 sediments (AOM, SBR, MG), they are commonly separated in the sedimentary column, methanogenesis
397 being deeper than SBR. However, co-occurrence of SBR and methanogenesis associated to modern whale

carcasses has been demonstrated by Treude et al. (2009) and reported also by Smith et al., 2015. Therefore, their discrimination in fossil material is hard throughout a petrographic approach.

It is a matter of fact that the soft tissues of the marine vertebrates represent a high amount of organic matter available for decomposing agents (Smith, 2006), able to influence also the surrounding sediment (Smith and Baco, 2003; Treude et al., 2009), thus it may be questioned why dolomite formation did not occur before the bones were covered by the sediment. Dolomite formation may have been inhibited in the very early stages of soft tissue decay due to possible oxic degradation promoting acidic conditions, unfavourable for carbonate mineral precipitation (Coleman, 1993). It cannot be excluded that the presence of a high amount of biomass may have favoured nodule formation: the presence microrganisms related to its decay changed the geochemical conditions of the surrounding sediments favouring alkaline conditions and carbonate nucleation, as suggested by Bontognali et al. (2014) based on experimental results. However, dolomite formed when soft tissues were decayed and the bones cavities were filled by sediment: this evidence strongly suggests that dolomite precipitation is mainly ruled by the presence of of bones lipids rather than by that of soft tissues. This is in agreement with the observations and the degradation rate assessment reported by several authors, suggesting that the utilization of bone lipids by sulphate-reducing bacteria is much slower and sustained compared to the soft tissues consumption (Schuller et al., 2004; Treude et al., 2009). Therefore, bone lipids represent a source of organic matter available for degradation after skeletonization and sediment infilling (e.g. endocranium).

Petrographic textures similar to those presented here have been described by several authors (Kaim et al., 2008; Kiel, 2008; Shapiro and Spangler, 2009; Danise et al., 2012). Based on carbon isotope similarity, Kiel (2008) suggests that the carbonate cements inside the bones and the external concretions formed at the same time, and proposes that they formed thousands of years after the death of the whale, therefore unrelated to the bone lipids degradation. On the other hand, Shapiro and Spangler (2009) note the lack of cement in the central cancellous bone and take it as an evidence against later pore water circulation, preferring the microbial origin. For what the studied Ica desert concretions are concerned, the field and petrographic evidence collected in this work indicate that the dolomite within bone cavities formed during the same process that lead to the outer concretions. Unlike Kiel's reconstruction, this contemporaneity can be an

425 evidence that both in the bones and in the external nodules, carbonate formation was related to lipids
426 degradation operated by bacteria.

427 Our results allow to contribute to the comparison between the processes and timing observed at present
428 in deep and shallow sea whale-falls (Deming et al., 1997; Smith and Baco, 2003; Little, 2010; Smith et al.,
429 2015) and their fossil equivalent (e.g. Dominici et al., 2009; Danise et al., 2012). The first stage of the
430 whale's decomposition is the mobile-scavenger stage, with sharks and crabs eating all the soft tissues for a
431 couple of years (Smith and Baco, 2003). The next stage (the enrichment-opportunist stage, shorter than two
432 years, as described by Smith and Baco, 2003) involves "dense assemblages of heterotrophic macrofauna
433 (especially polychaetes and crustaceans)", which "colonize the bones and organically enriched sediments
434 surrounding the carcass" (Smith et al., 2015). The third stage is the sulphophilic stage: anaerobic bacteria
435 exploiting the lipids in the bone reduce SO_4^{2-} and release H_2S, which is oxidized by the sulphophilic bacteria
436 using sea water oxygen. In this stage a large community of mussels, clams and limpets thrives by exploiting
437 sulphide-based chemoautotrophic production for up to fifty years (Smith and Baco, 2003). During this stage
438 also methane can be released from the decaying tissue and bacterial methanothrophs may thrive (Smith et al.,
439 2015). The final stage is the reef stage, during which the mineral remains of the skeleton are colonized by
440 suspension feeders (Smith et al, 2015).

441 Evidence of the occurrence of a sulphide-based chemoautotrophic community have been commonly
442 found in association to whale falls in the fossil records for deep sea and outer shelf (Amano and Little, 2005;
443 Danise et al., 2010; Dominici et al., 2009). In shallow shelves and coastal settings, fossil traces of bone
444 degradation due to microbial activity have been documented (Dominici et al., 2009; Shapiro and Spangler,
445 2009; Danise et al., 2012. Danise et al. (2012) found, on a shallow fossil whale fall, traces of pre-burial
446 activity (microborings, traces of iron sulphides testifying sulphate reduction), dolomite concretions formed
447 after burial during bone lipids degradation, but no trace of chemosynthetic invertebrates testifying the
448 development of a sulphide-based chemoautotrophic ecosystem (Danise et al., 2012). Rare fossil
449 chemosynthetic bivalves were instead found by Danise and Dominici, 2014. Also in our case, evidence of
450 this molluscan community are scarce; in addition, because of the lack of hinges due to bad conservation of
451 bivalves, the chemosynthetic nature of those molluscs associated to Cerro Los Quesos carcasses could be

452 speculated only by their position with respect to fossils (see Table S2, supplementary material and Fig. S3,
453 supplementary material). The fossils with associated bivalves (CLQ-C46, CLQ-C47, CLQ-O7) are all
454 positioned on the same stratigraphic level. Our reconstruction of nodule formation mechanisms suggests that
455 the geochemical condition in which nodule developed was suitable for the flourishing of the sulphophilic
456 stage community observed at modern whale-falls. Therefore, the prevailing absence of chemosynthetic
457 bivalve traces must be ascribable to different causes that prevented their flourishing or their preservation.
458 Overall we propose that organic matter decay processes were able to sustain a long-lived biomineralization
459 factory that lead to the formation of the dolomitic nodules.
460
461 *5.2 The boundary between concretions and unaffected sediment*
462
463 With or without dolomite concretions, the presence of the YBR sequence in correspondence to fossil
464 remains is recurrent; this fact made us suspect that its formation was closely related to the reduced
465 environmental conditions induced by carcasses degradation, just as much as the dolomite is.
466 The yellow layer surrounds the dolomite nodule or is directly in contact with the bones, but dolomite is
467 rarely found or completely absent from it (see paragraph 4.2.2). Therefore, we suggest that it represents an
468 incipient phase of nodule formation. When fossils are mostly complete and articulated but lie directly on the
469 yellow layer, bicarbonate saturation may have been inhibited by different causes (i.e. sulphate penetration
470 throughout the sediment porosity), preventing the precipitation of high amounts of dolomite. Moreover, the
471 environment around the bones was undergoing enhanced reduced conditions compared to the surrounding
472 sediments, strongly influencing the behaviour of redox-sensitive elements. This allowed the Fe (dissolved in
473 pore water after iron reduction, or derived from terrigenous as well as from organic matter) to be fixed as
474 sulphides. Similarly, reduced conditions increased Mn solubility, allowing it to form solubile compounds
475 with humic acids; on the other hand oxidation causes the formation of insoluble organic manganese
476 compounds (López-González et al., 2006). Biologically-induced Mn reduction exploited Mn particulate
477 present in the oxygenated sea water and Mn contained in the volcanogenic sediment particles. A redox
478 discontinuity layer formed where the reducing conditions ceased, causing the precipitation of Mn species and

479 the oxidation of Fe, that makes the sediment color turning into red. Migration of Mn by diffusion in
480 obedience of the redox gradient is suggested by the texture of the Mn-rich black layers. We infer that the
481 YBR sequences mark the outer boundaries of the volume of sediment where reducing conditions were
482 induced by organic matter decay, thus favouring the concentration of redox-sensitive elements as Fe and Mn,
483 in an overall oxic sea bottom (as also highlighted by Treude et al., 2009). Although this sequence was only
484 found below fossil specimens, we cannot exclude that it completely surrounded fossils and that it was eroded
485 by recent weathering agents.
486
487 *5.3 Factors affecting the extent of dolomitic nodules formation*
488
489 Many factors might control the degree of dolomite development around the vertebrate skeletons in the
490 Pisco Fm. Basically, the microbially mediated dolomite formation requires removal of sulphate ions
491 inhibiting primary dolomite (Baker and Kastner, 1981), joined to carbonate supersaturation caused by the
492 increase in alkalinity from bacterial degradation of organic matter (Claypool and Kaplan, 1974; Compton,
493 1988a): any variation of these requirements may interrupt the process of dolomite cement formation. Some
494 factors affecting these variables are discussed here below.
495 (i) The available amount of biomass affects the extent of time during which bacterial degradation occurs
496 and the volume of sea bottom sediment affected (Smith, 2006; Treude et al., 2009). Large carcasses furnish a
497 large amount of organic matter and allow anaerobic degradation to begin in the interior, while aerobic decay
498 acts on tissues exposed to oxygenated bottom waters. Although dolomite formation occurred after
499 consumption of soft tissues, we cannot exclude that the huge amount of biomass conditioned the sediment
500 surrounding carcasses (Smith and Baco, 2003; Treude et al., 2009; Bontognali et al., 2014). The positive
501 relationship between nodule formation and biomass amounts is clearly supported by field-data (Fig. 4C).
502 Indeed, nodules mostly wrap: 1) fossils of larger size (basically mysticetes, fig. 4C); 2) highly articulated and
503 highly complete skeletons (Fig. 4D and 4E), these two properties being directly related to the amount of
504 bones and flesh that reached the sea bottom with the skeletons.

505 (ii) Once the soft tissues have gone, the amount of bone lipids available for degradation could affect the
506 chemical environment of the skeleton. Higgs et al. (2011) documented that: 1) bones from different parts of
507 the skeleton have different lipid content; 2) lipids content increases with body size. Accordingly, we nearly
508 always found dolomite concretions between vertebrae (lumbar vertebrae) and as endocranial nodules. Also
509 nodule prevail around mysticetes than around odontocetes (Fig. 4C).
510 (iii) The persistence of low sulphate conditions is unfavoured by the continuous availability of sulphate
511 from the oxygenated bottom waters, even if the environment close to the decaying carcass is reduced. From
512 our data, it seems as if the formation of nodules required the bones buried in the sediment before the
513 exhaustion of bone lipids. It could be proposed that early covering by sediments allowed the isolation from
514 the oxygenated waters required to maintain the conditions for carbonate precipitation. A highly porous
515 sediment (highly permeable) may alter this condition, favouring the exchange of sulphate with bottom
516 waters.
517 No relationship seems to exists between the nodules formation and their distribution in space and time
518 within the Pisco Fm. Although stratigraphic layers of dolomite are commonly present within the vertical
519 development of the sequence, nodules distribution is unrelated to those and to any other stratigraphic
520 horizon. Continuous layers of dolomite were likely formed at the sulphate–methane interface within the
521 sedimentary column due to alkalinity increase related to microbial activity degrading organic carbon-
522 (Compton, 1988b; Meister et al., 2008), most likely deeper (within the first 30 m) in the sedimentary column
523 compared to depth of nodules formation. For what lithologies are concerned, fossils at Cerro Colorado seem
524 to prevail in diatomite and in diatomaceous sandstone rather than in fine-grained sand (Bianucci et al., 2015).
525 However, this fact may be attributed to the scarcity of this latter lithology within the Cerro Colorado
526 sequence (Di Celma et al., 2015). Likewise, the nodules that we analysed are not preferentially located in one
527 lithology or the other. Therefore, nodule formation is not assignable to a specific or recurrent event in the
528 stratigraphic record, neither to a given sedimentation rate (as this cannot be assumed constant throughout the
529 different lithologies), but rather to recurrent specific geochemical conditions at the local scale.
530
531 *5.4 Role of the presence/absence of dolomitic nodules in the formation of the Pisco Lagerstätte.*

532

533 The formation of dolomite nodules preserves bones at the outcrop as long as the nodule is intact.
534 However, the nodule formation may limit or prevent the complete remineralization of the bones, reducing
535 bones resistance to erosion agents when exposed. Indeed, bones originally wrapped up in nodules are
536 delicate and brittle if exposed to weathering: this suggests that they underwent scarce or no remineralization.
537 The bone structures, such as osteons, trabeculae and Haversian canals, are very well preserved.

538 On the other hand, the lowering of sediment permeability concomitant to the formation of the
539 concretions, could have allowed the preservation of very labile structures or rapidly degrading tissues, as
540 discussed by McCoy et al. (2015). This could be the reason for the exeptional preservation of baleen in the
541 Pisco Fm. Described by Esperante et al. (2008). Besides the current role of nodules in protecting the bones at
542 the outcrop, our reconstruction of the timing and mechanisms of their formation during early diagenesis
543 implies additional ways through which they acted a central role in the preservation of the Pisco marine fossil
544 vertebrates:

545 • the early stage of nodules formation presupposes an increase of alkalinity, consequent to microbial
546 activity, that avoided the dissolution of bones;
547 • early filling and cementation of skeletal voids prevented diagenetic compression of specimens (as
548 occurred, on the contrary, in the case of the holotype of *Nazcacetus urbinai* Lambert et al, 2009);
549 • nodules worked as a protection against any erosive events that may have acted in case of re-
550 exposition of the fossils on the sea floor;
551 • since the formation of nodules was favored by large size, articulation and completeness of the
552 remains, the Pisco nodules had a role in preserving complete and articulated specimens;
553 • finally, in some cases, the formation of the dolomite nodules could have contributed to the
554 preservation of very labile structures or tissues, lowering sediment permeability.

555 Therefore, the formation of the concretions contributed in different ways to the development of the Pisco
556 Lagerstätte.

557

558 **6. Conclusions**

559

560 In the Pisco renown fossil vertebrate deposit (Ica desert), field investigations and petrographic results
561 indicate a strict correspondence between the presence of the isolated dolomite nodules and the remains of
562 fossil vertebrates. This correspondence, together with the positive relationships between size, completeness
563 and articulation of skeletons and the presence of an external nodule, support a cause-effect relation.
564 Dolomite formed shortly after the soft tissues decayed and the skeletons were covered by sediment. We
565 propose that the dolomite surrounding the fossils of the Pisco Fm. was precipitated mostly because of
566 microbially mediated processes (methanogenesis and sulphate reduction), during bone lipid degradation. Iron
567 hydroxides maintaining the texture of pyrite framboids are evidence of sulphide production during dolomite
568 precipitation, while clotted dolomite and microborings are evidence of microbial activity in correspondence
569 of bones. Field results relate nodule development with size, completeness and articulation of fossils: this
570 evidence can be taken as proof that an intense and prolonged bacterial activity related to a higher amounts of
571 lipid favored the formation of the nodules. We suggest that this activity is operated by the same bacteria
572 operating during stage three of whale-fall communities and that vertebrate wrapped up in partial or complete
573 nodules can be identified as fossil and partially-developed whale fall communities. We suggest that an early
574 burial by sediment was a determinant factor in the development of dolomite concretions, since it allowed
575 anaerobic degradation processes before lipid exhaustion. Rapid burial was favored by the carcasses sinking
576 into an unconsolidated sediment.
577 A characteristic sequence of redox-sensitive elements enrichment (Mn, Fe) under or around the fossils is
578 interpreted as a consequence of the reducing conditions in the sediment surrounding the carcasses, differing
579 from the general geochemical conditions of the sea-bottom.
580 Although not all the fossils of the Pisco Fm. are interested by nodules, we suggest that dolomitic nodules
581 played a central role in the development of the Pisco Lagerstätte, acting throughout different protection
582 mechanisms: increase of alkalinity in the early stage of nodule formation avoided the dissolution of bones;
583 early diagenetic formation of nodules limited erosive agents on the sea floor (such as bottom currents); early
584 filling and cementation of skeleton voids prevented diagenetic compression of specimens; lowering of
585 sediment permeability in some cases contributed to the preservation of very labile structures or tissues.

586 Moreover, the formation of nodules was favored by large size, articulation and completeness of the fossil
587 vertebrates. Therefore, the nodules had a role in the preservation of complete and articulated specimens, thus
588 favoring the formation of the exceptional Pisco Lagerstätte.
589
590 **Aknowledgment**
591
592 We thank Olivier Lambert (Département de Paléontologie, Institut Royal des Sciences Naturelles de
593 Belgique) for his great help and assistance in the field; Carlo Gini and Cristian Biagioni (Dipartimento di
594 Scienze della Terra, Università di Pisa) for the help in realizing and interpreting XRDP analyses; Daniela
595 Basso (DISAT, Università di Milano-Bicocca) for fruitful discussions on bivalves ecology. We also would
596 like to thank two anonymous reviwers for all the corrections and suggestions that helped improving the
597 manuscript. This research was supported by a grant of the Italian Ministero dell'Istruzione dell'Università e
598 della Ricerca (PRIN Project 2012YJSBMK) and by a National Geographic Society Committee on Research
599 Exploration grant (9410-13) to G. Bianucci.
600
601 **References**
602 Allison P.A., 1988a. The decay and mineralization of proteinaceous macrofossils. Paleobiology, 14:139-154.
603 Allison, P.A., Smith, C.R., Kukert, H., Deming, J.W., Bennett, B.A., 1991. Deep-water taphonomy of
604 vertebrate carcasses: a whale skeleton in the bathyal Santa Catalina Basin. Paleobiology, 17: 78-89.
605 Aloisi, G., Pierre, C., Rouchy, J. M., Foucher, J. P., & Woodside, J., 2000. Methane-related authigenic
606 carbonates of eastern Mediterranean Sea mud volcanoes and their possible relation to gas hydrate
607 destabilisation. Earth and Planetary Science Letters, 184(1): 321-338.
608 Amano, K., & Little, C. T., 2005. Miocene whale-fall community from Hokkaido, northern Japan.
609 Palaeogeography, Palaeoclimatology, Palaeoecology, 215(3):345-356.
610 Baker, P. A., Kastner, M., 1981. Constraints on the formation of sedimentary dolomite. Science, 213(4504):
611 214-216.

612 Berner, R.A., 1968. Calcium Carbonate Concretions Formed by the Decomposition of Organic Matter.
613 Science 159(3811): 195-197.
614 Berner, R.A., 1970. Sedimentary pyrite formation. American Journal of Science, 268: 1-23.
615 Berner, R.A., 1984. Sedimentary pyrite formation: an update. Geochimica et Cosmochimica acta, 48(4): 605-
616 615.
617 Bernoulli, D., Gunzenhauser B., 2001. A dolomitized diatomite in an Oligocene-Miocene deep-sea fan
618 succession, Gonfolite Lombarda Group, Northern Italy. Sedimentary Geology, 139:71-91.
619 Bianucci, G., Lambert, O., Post, K., 2010. High concentration of long-snouted beaked whales (Genus
620 *Messapicetus*) from the Miocene of Peru. Palaeontology, Vol. 53(5):1077–1098.
621 Bianucci, G., Di Celma, C., Landini, W., Post, K., Tinelli, C., de Muizon, C., Gariboldi, K., Malinverno, E.,
622 Cantalamessa, G., Gioncada, A., Collareta, A., Salas-Gismondi, R., Varas-Malca, R., Urbina, M.,
623 Lambert, O., 2015. Distribution of fossil marine vertebrates in Cerro Colorado, the type locality of the
624 giant raptorial sperm whale *Livyatan melvillei* (Miocene, Pisco Formation, Peru). Journal of Maps,
625 DOI:10.1080/17445647.2015.1048315.
626 Bodzioch, A., Kowal-Linka, M., 2012. Unraveling the origin of the Late Triassic multitaxic bone
627 accumulation at Krasiejów (S Poland) by diagenetic analysis. Palaeogeography, Palaeoclimatology,
628 Palaeoecology 346-347:25–36
629 Bojanowski, M. J., Clarkson, E. N. 2012. Origin of Siderite Concretions In Microenvironments of
630 Methanogenesis Developed In A sulphate Reduction Zone: An Exception Or A Rule?. Journal of
631 Sedimentary Research, 82(8):585-598.
632 Bontognali, T.R.R., McKenizie J.A., Warthmann, R.J., Vasconcelos, C., 2014. Microbially influenced
633 formation of Mg-calcite and Ca-dolomite in the presence of exopolymeric substances produced by
634 sulphate-reducing bacteria. Terra Nova 26: 72-77.
635 Brand, L., Urbina, M., Chadwick, A., DeVries, T.J., Esperante, R., 2011. A high resolution stratigraphic
636 framework for the remarkable fossil cetacean assemblage of the Miocene/Pliocene Pisco Formation, Peru.
637 Journal of South American Earth Sciences, 31: 414-425.

638 Briggs, D.E.G., 2003. The role of decay and mineralization in the preservation of soft-bodied fossils. Annual
639 Review of Earth Planetary Sciences, 31: 275-301.
640 Burne, R.V., Moore, L.S., 1987. Microbialites: organosedimentary deposits of benthic microbial
641 communities. Palaios 2:241–254.
642 Canfield, D.E,. Raiswell, R., 1991 Carbonate precipitation and dissolution: its relevance to fossil
643 preservation. In: Taphonomy: Releasing the data locked in the fossil record. P.A. Allison, P. A., Briggs,
644 D.E.G. (Eds.). Geobiology, 9, Plenum Press, New York, pp. 337-387.
645 Claypool, G.E., Kaplan, I.R., 1974. The origin and distribution of methane in marine sediments. In Natural
646 gases in marine sediments, by Kaplan I.R. (Ed.), pp 99-139, Plenum Press, New York.
647 Cobbing, E.J. , 1999. The Coastal Batholith and other aspects of Andean magmatism in Peru. In: Castro, A.,
648 Fernandez, C. & Vigneresse, J.L. (Eds.), Understanding Granites: Integrating New and Classical
649 Techniques. Geological Society, London, Special Publications, 168:111–122.
650 Coleman, M.L., 1993. Microbial processes: Controls on the shape and composition of carbonate concretions.
651 Marine Geology, 119: 127-140.
652 Compton, J.S., 1988a. Degree of supersaturation and precipitation of organogenic dolomite. Geology, 16(4):
653 318-321.
654 Compton, J.S., 1988b. Sediment composition and precipitation of dolomite and pyrite in the Neogene
655 Monterey and Sisquoc Formations, Santa Maria Basin area, California. In: Shukla, V., Baker, P.A. (Eds.),
656 Sedimentology and Geochemistry of Dolostones. SEPM Spec. Pub., Tulsa, vol. 43: 53–64.
657 Danise, S., Dominici, S., Betocchi, U., 2010. Mollusk species at a Pliocene shelf whale fall (Orciano Pisano,
658 Tuscany). Palaios, 25(7):449-456.
659 Danise, S., Dominici, S., 2014. A record of fossil shallow-water whale falls from Italy. Lethaia: 47:229-243.
660 Danise, S., Calvazzi, B., Dominici S., Westall, F., Monechi, S., Guioli S., 2012. Evidence of microbial
661 activity from a shallow water whale fall (Voghera, northern Italy). Palaeogeography, Palaeoclimatology,
662 Palaeoecology 317-318:13-26.Danise, S., Twitchett, R. J., & Matts, K., 2014. Ecological succession of a
663 Jurassic shallow-water ichthyosaur fall. Nature communications, 5.

664 Davis, P.G., 1997. The bioerosion of bird bones. International Journal of Osteoarchaeology 7:388-
665 401.
666 Deming, J.W., Reysenbach, A.L., Macko, S.A., Smith, C.R., 1997. Evidence for the microbial basis of a
667 chemoautotrophic invertebrate community at a whale fall on the deep seafloor: bone-colonizing bacteria
668 and invertebrate endosymbionts. Microscopy Research and Technique, 37(2):162–170.
669 DeVries, T. J., 1988. Paleoenvironments of the Pisco Basin. Cenozoic Geology of the Pisco Basin. In
670 Cenozoic Geology of the Pisco Basin. Guidebook, IGCP 156 Field Workshop: Genesis of Cenozoic
671 Phosphorites and Associated Organic-rich sediments: Peruvian Continental Margin, Dunbar, R.B. and
672 Baker, P.A. (pp. 41-50).
673 Di Celma C., Malinverno E., Gariboldi K., Gioncada A., Rustichelli A., Pierantoni, P.P., Landini W., Tinelli,
674 C., Bianucci G., 2015. Stratigraphic framework of the late Miocene to Pliocene Pisco Formation at Cerro
675 Colorado (Ica Desert, Peru). Journal of Maps, DOI: 10.1080/17445647.2015.1047906
676 Di Celma C., Malinverno E., Cantalamessa G., Gioncada A., Bosio G., Villa I., Gariboldi K., Rustichelli A.,
677 Pierantoni P.P., Landini W., Tinelli C., Collareta A., Bianucci G., submitted. Stratigraphic framework of
678 the late Miocene Pisco Fm. (Ica Desert, Peru). Journal of Maps.
679 Dominici, S., Cioppi, E., Danise, S., Betocchi, U., Gallai, G., Tangocci, F., Valleri, G., Monechi, S., 2009.
680 Mediterranean fossil whale falls and the adaptation of mollusks to extreme habitats. Geology, 37(9):815–
681 818.
682 Dunbar, R.B., Marty, R.C., Baker, P.A., 1990. Cenozoic marine sedimentation in the Sechura and Pisco
683 basins, Peru. Palaeogeography, Palaeoclimatology, Palaeoecology 77:235-261.
684 Eggleston, C. M., Ehrhardt, J. J., & Stumm, W., 1996. Surface structural controls on pyrite oxidation
685 kinetics: an XPS-UPS, STM, and modeling study.American Mineralogist, 81(9):1036-1056.
686 Esperante, R., Brand, L., Nick, K., Poma, O., Urbina, M., 2008. Exceptional occurrence of fossil baleen in
687 shallow marine sediments of the Neogene Pisco Formation, Southern Peru. Palaeogeography,
688 Palaeoclimatology, Palaeoecology 257:344-360.Esperante, R., Brand, L.R., Chadwick, A.V., Poma, O.,
689 2015, Taphonomy and paleoenvironmental conditions of deposition of fossil whales in the diatomaceous

690 sediments of the Miocene/Pliocene Pisco Formation, southern Peru—A new fossil-lagerstätte.
691 Palaeogeography, Palaeoclimatology, Palaeoecology 417:337–370.
692 Ehret, D. J., MacFadden, B. J., Salas-Gismondi, R. , 2009. Caught in the act: Trophic interactions between a
693 4-million-year-old white shark (Carcharodon) and mysticete whale from Peru. Palaios,24(5):329-
694 333.Goffredi, S. K., Paull, C. K., Fulton-Bennett, K., Hurtado, L. A., & Vrijenhoek, R. C., 2004. Unusual
695 benthic fauna associated with a whale fall in Monterey Canyon, California. Deep Sea Research Part I:
696 Oceanographic Research Papers, 51(10):1295-1306.
697 Higgs, N.D., Little, C.T.S., Glover, A.G., 2011 Bones as biofuel: a review of whale bone composition with
698 implications for deep-sea biology and paleoanthropology. Proceedings of the Royal Society B 278: 9-17.
699 Higgs, N. D., Glover, A. G., Dahlgren, T. G., Smith, C. R., Fujiwara, Y., Pradillion, F., Johnson, S.B.,
700 Vrijenhoek, R.C., & Little, C. T., 2014. The morphological diversity of *Osedax* worm borings (Annelidia:
701 Siboglinidae). Journal of the Marine Biological Association of the United Kingdom, 94(7):1429-1439.
702 Hsu, J.T., 1992. Quaternary uplift of the Peruvian Coast related to the subduction of the Nazca Ridge: 13.5 to
703 15.6 degrees South Latitude. Quaternary International 15-16:87-97.
704 Irwin, H., Curtis, C., Coleman, M., 1977. Isotopic evidence for source of diagenetic carbonates formed
705 during burial of organic-rich sediments. Nature 27: 577-591
706 Jinhua, L., Benzeraraa, K., Bernardb, S., Beyssaca, O., 2013. The link between biomineralization and
707 fossilization of bacteria: Insights from field and experimental studies Chemical Geology, 359:49–69
708 Jørgensen, N.O.,1992. Methane-derived carbonate cementation of marine sediments from the Kattegat,
709 Denmark: geochemical and geological evidence.Marine Geology, 103(1): 1-13.
710 Kaim, A., Kobayashi, Y., Echizenya, H., Jenkins, R.G., Tanabe, K., 2008. Chemosynthesis based
711 associations on Cretaceous plesiosaurid carcasses. Acta Palaeontologica Polonica 53:97–104
712 Kelts, K., McKenzie, J., 1984. A comparison of anoxic dolomite from deep-sea sediments: Quaternary Gulf
713 of California and Messinian Tripoli formation of Sicily. In: Garrison, R.E., Kastner, M., Zenger, D.H.
714 (Eds.) , Dolomites of the Monterey. Formation and Other Organic-Rich Units. Pacific Section S.E.P.M.,
715 Vol. 41: 19–28.

716 Kennard, J.M., James, N.P., 1986. Thrombolites and Stromatolites: Two Distinct Types of Microbial
717 Structures. Palaios, 1(5): 492-503.
718 Kiel S., 2008. Fossil evidence for micro- and macrofaunal utilization of large nektonfalls: examples from
719 early Cenozoic deep-water sediments in Washington State, USA. Palaeogeography, Palaeoclimatology,
720 Palaeoecology 267:161–174.
721 Kiel, S., Goedert. J.L., Kahl, W.A., Rouse, G.W., 2010. Fossil traces of the bone –eating worm *Osedax* in
722 early Oligocene whale bones. Proceedings of the National Academy of Sciences, 107(19):8656-8659.
723 Kiel, S., Goedert. J.L., Kahl, W.A., 2013. Traces of the bone-eating annelid *Osedax* in Oligocene whale teeth
724 and fish bones. Paläontologische Zeitschrift, 87(1):161-167.
725 Kulm, L.D., Suess, E., Thornburg, T.M., 1984. Dolomites in the organic-rich muds of the Peru forearc
726 basins: analogue to the Monterey Formation. In Garrison, R.E., Kastner, M., and Zenger, D.H. (Eds.),
727 Dolomites of the Monterey. Formation and Other Organic-Rich Units. Pacific Section S.E.P.M.,,
728 Vol. 41: 29-48.
729 Lambert, O., Bianucci, G., de Muizon, C., 2008. A new stem-sperm whale (Cetacea, Odontoceti,
730 Physeteroidea) from the Latest Miocene of Peru. Comptes Rendus Palevol, 7:361–369.
731 Lambert, O., Bianucci, G., Post, K., 2009. New beaked whale (Odontoceti, Ziphiidae) from the middle
732 Miocene of Peru. Journal of Vertebrate Paleontology, 29(3):910–922.
733 Lambert, O., Bianucci, G., Post, K., de Muizon, C., Salas-Gismondi, R., Urbina, M., Reumer, J., 2010. The
734 giant bite of a new raptorial sperm whale from the Miocene epoch of Peru. Nature, 466:105-108.
735 Lambert, O., De Muizon, C., Bianucci, G., 2013. The most basal beaked whale *Ninoziphius platyrostris*
736 Muizon, 1983: clues on the evolutionary history of the family Ziphiidae (Cetacea: Odontoceti).
737 Zoological Journal of the Linnean Society, 167: 569–598.
738 Little, C.T.S., 2010. The prolific afterlife of whales; on the deep seafloor, the carcasses of the largest
739 mammals give life to unique ecosystems. Scientific American 302:78 – 84.
740 López-González, F., Grandal-d'Anglade, A., Vidal-Romaní, J.R., 2006. Deciphering bone depositional
741 sequences in caves through the study of manganese coatings. Journal of Archological Science 33:707-717

742 Luff, R., & Wallmann, K., 2003. Fluid flow, methane fluxes, carbonate precipitation and biogeochemical
743 turnover in gas hydrate-bearing sediments at Hydrate Ridge, Cascadia Margin: numerical modeling and
744 mass balances.Geochimica et Cosmochimica Acta, 67(18) :3403-3421.
745 McCoy, V.E., Young, R.T., Briggs, D.E.G., 2015. Factors controlling exceptional preservation in
746 concretions. Palaios 30:272-280
747 Meister, P., McKenzie, J.A., Warthmann, R., Vasconcelos, C., 2006. Mineralogy and petrography of
748 diagenetic dolomite from the ODP Leg 201 Peru margin drill sites. Proc. ODP, Sci. Results.
749 Meister, P., Mckenzie, J. A., Vasconcelos, C., Bernasconi, S., Frank, M., Gutjahr, M., Schrag, D. P., 2007.
750 Dolomite formation in the dynamic deep biosphere: results from the Peru Margin. Sedimentology,
751 54(5):1007-1032.
752 Meister, P., Bernasconi, S. M., Vasconcelos, C., McKenzie, J. A., 2008. Sealevel changes control diagenetic
753 dolomite formation in hemipelagic sediments of the Peru Margin.Marine Geology, 252(3):166-173.
754 Meister, P., Gutjahr, M., Frank, M., Bernasconi, S. M., Vasconcelos, C., & McKenzie, J. A., 2011. Dolomite
755 formation within the methanogenic zone induced by tectonically driven fluids in the Peru accretionary
756 prism. Geology, 39(6):563-566.
757 Meister, P., 2013. Two opposing effects of sulfate reduction on carbonate precipitation in normal marine,
758 hypersaline, and alkaline environments. Geology, 41(4):499-502.
759 Montoya, M., García, W., Caldas, J., 1994. Geologia de los cuadrangolos de Lomitas, Palpa, Nasca y Puquio.
760 Republica del Peru, Sector Energia y Minas, Instituto Geologico y Minero y Metalurgico, 53(A).
761 Moore, T. S., Murray, R. W., Kurtz, A. C., Schrag, D. P., 2004. Anaerobic methane oxidation and the
762 formation of dolomite. Earth and Planetary Science Letters, 229(1):141-154.
763 Muizon, C. de, DeVries, T.J., 1985. Geology and paleontology of late Cenozoic marine deposits in the
764 Sacaco area (Peru). Geologische Rundschau, 74:547–563
765 Mukasa, S.B., 1986. Zircon U–Pb ages of super-units in the Coastal batholith, Peru: implications
766 for magmatic and tectonic processes. Geological Society of America Bulletin, 97:241–254.

767 Pike, J., Bernhard, J.M., Moreton, S.G., Butler, A.B., 2001. Microbioirrigation of marine sediments in
768 dysoxic environments: implication for early diagenetic sediment fabric formation and diagenetic
769 processes. Geology, 29(10):923-926.
770 Riding, R., 2000. Microbial carbonates: the geological record of calcified bacterial–algal mats and biofilms.
771 Sedimentology, 47(1): 179–214.
772 Riding, R., Tomás, S, 2006. Stromatolite reef crusts, Early Cretaceous, Spain: bacterial origin of in situ-
773 precipitated peloid microspar?. Sedimentology, 53:23-24.
774 Romero, D., Valencia, K., Alarcón, P., Peña, D., Ramos, V.A., 2013. The offshore basement of
775 Perú: Evidence for different igneous and metamorphic domains in the forearc. Journal of South
776 American Earth Sciences, 42:47–60.
777 Schuller, D., Kadko, D., Smith, C.R., 2004 Use of $^{210}Pb/^{226}Ra$ disequilibria in the dating of deep-sea whale
778 falls. Earth and Planetary Science Letters 218:277-289
779 Seilacher, A., 1970. Begriff und bedeutung der Fossil-Lagerstätten. Neues Jahrbuch für Geologie und
780 Paläontologie Abhandlungen, (1):34-39.
781 Shapiro, R.S., Spangler, E., 2009. Bacterial fossil record in whale-falls: petrographic evidence of microbial
782 sulfate reduction. Palaeogeography, Palaeoclimatology, Palaeoecology 274:196-203.
783 Smith, C.R., 2006. Bigger is better: the role of whales as detritus in marine ecosystems. In: Estes, J.A.,
784 DeMaster, D.P., Brownell Jr., R.L., Doak, D.F., Williams, T.M. (Eds.), Whales, Whaling and Ocean
785 Ecosystems. University of California Press, Berkeley, CA, USA, pp. 286–301.
786 Smith, C.R., Baco, A.R., 2003. Ecology of whale falls at the deep-sea floor. Oceanography and Marine
787 Biology: an Annual Review, 41:311–354.
788 Smith, C. R., Glover, A. G., Treude, T., Higgs, N. D., & Amon, D. J., 2015. Whale-Fall Ecosystems: Recent
789 Insights into Ecology, Paleoecology, and Evolution. Marine Science,7:571-596.
790 Suess, E., von Huene, R., 1988. Introduction, objectives, and principal results, Leg 112, Peru continental
791 margin. Proc. Ocean Drilling Program, Init. Rep. Vol. 112:5-44.
792 Tarr, W.A., 1921. Syngenetic origin of concretions in shale. Geological Society of America Bulletin,
793 32(4):373-384.

794 Teal, C. S., Mazzullo, S. J., & Bischoff, W. D., 2000. Dolomitization of Holocene shallow-marine deposits
795 mediated by sulfate reduction and methanogenesis in normal-salinity seawater, northern Belize. Journal
796 of Sedimentary Research, 70(3):649-663.
797 Thornburg, T.M., & Kulm, L.D., 1981. Sedimentary basins of the Peru continental margin: structure,
798 stratigraphy, and Cenozoic tectonics from 6ºS to 16º latitude. In: Kulm, L.D., Dymond, J., Dasch, E.J., &
799 Hussong, D.M. (Eds.), Nazca plate: crustal formation and Andean convergence. Geological Society of
800 America, Memoir 154:393–422
801 Treude, T., Smith, C.R., Wenzhöfer, F., Carney, E., Bernardino, A., Hannides, A.K., Krüger, M., Boetius,
802 A., 2009. Biogeochemistry of a deep-sea whale fall: sulfate reduction, sulfide efflux and methanogenesis,
803 Marine Ecology Progress Series, 382:1–21.
804 Van Lith, Y., Warthmann, R., Vasconcelos, C., McKenzie, J.A., 2003. Microbial fossilization in carbonate
805 sediments: a result of the bacterial surface involvement in dolomite precipitation. Sedimentology 50:237–
806 245.
807 Vasconcelos, C., McKenzie, J.A., Bernasconi, S., Grujic, D., Tien, A.J., 1995. Microbial mediation as a
808 possible mechanism for natural dolomite formation at low temperatures. Nature 377: 220-222.
809 Weeks, L.G. 1957. Origin of carbonate concretions in shales, Magdalena Valley, Colombia. Geological
810 Society of America Bulletin, 68(1):95-102.

Table Caption changes marked

Table captions

Table 1. List of fossils specimens selected for laboratory analyses. These specimens are representative of the range of nodule development.~~,~~ T~~t~~heir main field characteristics, taphonomic aspects, samples description~~ing and~~ and type of analysis are tabulated..

Table 2. Representative major element composition (wt%) of the dolomitic concretions assessed by averaging several EDS analyses on 1x1 mm windows, with standard deviations (column 2 to 9). Representative composition (wt%) of zoned dolomite crystals within bone cavities (column 10 and 11).

Formatted: Line spacing: Double

Formatted: Numbering: Continuous

Table captions

Table 1. List of fossils specimens selected for laboratory analyses. These specimens are representative of the range of nodule development. Their main field characteristics, taphonomic aspects, samples description and type of analysis are tabulated..

Table 2. Representative major element composition (wt%) of the dolomitic concretions assessed by averaging several EDS analyses on 1x1 mm windows, with standard deviations (column 2 to 9). Representative composition (wt%) of zoned dolomite crystals within bone cavities (column 10 and 11).

Figure Caption changes marked

Figure captions

Formatted: Line spacing: Double

Formatted: Numbering: Continuous

Fig. 1. Geographic and geomorphological settings of the Ica desert. A. Sketch map of Peru, with location of the Ica desert. B. Location of the sites of investigation, Cerro Colorado and Cerro ~~los~~ Los Quesos. C. The landscape at Cerro Colorado, with a concretion hiding a vertebrate fossil skeleton standing in relief in the foreground. The hammer is circled in red for scale.

Fig. 2. Carbonatic nodules enclosing fossils, Pisco Fm. A. Skull and articulated mandibles of Cetotheriidae (Cetacea, Mysticeti, specimen CC-M22) (left); the skull, the mandibles and the postcranial skeleton (not visible in the photo) were hidden in a nodule, which was partially destroyed to reveal the bones. Bones are ~~evidenced~~ highlighted in yellow and the nodule in orange (right). B. Partially articulated skeleton including skull of Cetotheriidae CC-M18 (left); colors of bones and nodules (right) as in A. C. Complete articulated skeleton of small Cetotheriidae CC-M72 (left); colours of bones and nodule (right) as in A. D. Portion of rostrum of the holotype of the physeteroid *Livyatan melvillei* (Cetacea, Odontoceti, CC-O29) (left) and its position in the skull evidenced in ~~yellow~~ light blue (right). Dolomite (orange) precipitated only around the teeth. —E. Portion of articulated skeleton including skull of kentriodontid-like Delphinida (Cetacea, Odontoceti, CC-O4). Dolomite (orange) precipitated within the mesorostral groove, the endocranial, and the neural canals of the vertebrae. Although not visible in the figure, this specimens lies on a yellow sediment lying on a millimetric black Mn layer.

Fig. 3. Examples of fossils with partial or no concretions and of the enclosing sediment. A. Articulated skeleton of Balaenopteroidea (Cetacea, Mysticeti, CLQ-~~A124~~M58) with skull partially eroded. This specimen lies directly on the YBR sequence (see boxes). The lower dark grey layer is a volcanic ash bed (arrow). –B. Portion of articulated vertebral column of Balaenopteroidea (CLQ- M33~~A55~~) lying on the YBR sequence. C. Disarticulated skeleton (skull, mandible, vertebrae and rib) of Cetotheriidae (Cetacea, ~~Mysticete~~Mysticeti, CC-M21)

without nodule; the diatomaceous sediment is reddened by some undetermined alteration process.

Fig. 4. Nodules distribution in the Cerro Colorado fossil vertebrate assemblage. A. Distribution of the nodules in the fossil vertebrate assemblage examined in this work at Cerro Colorado, as a function of the position along the stratigraphy. The represented stratigraphic interval is the Lower Allomember ~~(Di Celma et al., 2015 in review)~~ where a higher concentration of fossils was found; red lines at the base and top of the section represent~~s~~ respectively the Pisco Fm.-Chilcatay Fm. angular unconformity ~~between the Pisco Fm. and the Oligo-Miocene Chilcatay Fm.~~ and the Pisco Fm. intraformational angular unconformity (Di Celma et al., 2015). Elevations are in respect to the base of the section. Red ellipses along the stratigraphic column represent nodular dolomitic layers unrelated to the presence of vertebrate remains. Concentration of fossil specimens between 40 m and 75 m is due to the better exposure of the strata within that interval at Cerro Colorado (Bianucci et al., 2015 ~~in review~~). B. Presence of well developed or partially developed concretions in the whole fossil assemblage (N=157) of Cerro Colorado. C, D, E. Nodules r~~R~~elationships with taxa, completeness and articulation.

Fig. 5. Sampling strategy. A. ~~Position of sampled~~Sampling of concretions and bones in a mysticete skeleton (specimen CLQ-M1 shown as example). B. Schematic section of a bone enclosed in a dolomitic nodule. Red rectangles show the position of oriented subsamples. C. Example of the use of oriented subsamples: ~~V~~variation of extent of dolomite filling in an external nodule were studied~~:~~. SEM-BSEI images and microanalytical informations from specimen CC-M22.

Fig. 6. SEM images and transmitted light microscope photographs of nodules thin sections. A. Dolomite infilling trabecular tissue of specimens CLQ-M~~A~~1 (transmitted light, plane nicols); forams and diatoms (arrowheads) are visible within the aphanotopic dolomitic cement. B. Diatom within the nodule of~~-~~ specimen CC-M85 (SEM-BSE). The silica of the frustules was not dissolved (white star in the box) and dolomite completely filled the areolae (black star in the box). C. Examples of iron oxide framboid, formerly sulphide (left) and iron hydroxides

Formatted: Italian (Italy)
Formatted: Italian (Italy)

filling a diatom frustule in the dolomite of specimen CC-M85 (right). D. Broken trabeculae rimmed by dolomite. ~~E. Cortical bone tissue of specimen CLQ-A121 is crowded with microborings type one. This type of borings can be associated to Fe oxides (inbox; diameter of the framboid is ca. 7 µm). F. A second type of microborings characterizes the cortical tissue of a vertebra of specimen CLQ-A179.~~ ~~G~~E. Dolomite crystals nucleated on the trabeculae before the sediment filled the voids of the trabecular tissue (specimen CLQ-MA~~1~~) (SEM-BSE). Arrows point the boundary between the dolomite rim and the filling (and dolomitized) sediment ~~H~~F. A detail of iron oxides (arrowheads) ~~-~~associated to the dolomite rim seen in (~~G~~E). ~~I~~G. An evident zoning in composition in the drusy dolomite is revealed by SEM-BSE images. ~~I~~H. Internal mould of diatom areolae made of Mn minerals (YBR of specimen CLQ-~~A180~~C67).

Fig. 7~~–~~. Effect of dolomite precipitation on diagenetic compaction. Comparison between (A) *Coscinodiscus* frustules in a dolomitized mudstone from a nodule and (B) in the diatomaceous mudstone far from any dolomitc concretion. Early precipitated dolomite (A) prevented frustules from being squeezed by the sedimentary load (B). Arrows facing each other point to valves of the same frustule.

Fig. 8. Different ~~T~~types of microborings characterizing the cortical tissue of fossil whales from the Pisco Fm. A. Type A associated to Fe oxides (arrows; diameter of the framboid is ca. 7 µm). B. Mi~~i~~croborings type B interesting the outer 50 µm of the cortical bone tissue of specimen CLQ-M10. C. Microborings type C characterize the cortical tissue of a vertebra of specimen CLQ-M67.

~~Fig. 7. Comparison between (A) *Coscinodiscus* frustules in a dolomitized mudstone from a nodule and (B) in the diatomaceous mudstone far from any dolomitc concretion. Early precipitated dolomite (A) prevented frustules from being squeezed by the sedimentary load (B). Arrows facing each other point to valves of the same frustule. Scale bars = 100 µm.~~

Fig. ~~8~~9. Dolomite formation reconstruction. A. Marine vertebrate deposited at the sea floor. ~~Refloat~~

Formatted: Not Highlight

Formatted: Indent: Hanging: 1.03 cm, Space After: 2.85 pt, Line spacing: Double

Formatted: Line spacing: Double

Formatted: Not Highlight

Formatted: Not Highlight

~~of carcasses due to decay gases likely occurred in the shallow waters of Cerro los Quesos and Cerro Colorado.~~ B. The consumption of the soft tissue is rapid (a few years, Treude et al., 2009) compared to lipid degradation. The skeleton was rapidly buried (see paragraph 5.1 for explanation). Rapid burial affected the skeleton. Sulphate reducing bacteria are represented: these could be closely related to the sulphate-reducing organisms of the whale-fall sulphophilic stage (lasting from 2 to 50~~1~~ yrs, Smith and Baco 2003). The mobile scavenger stage and the enrichment opportunist stage are not represented because we found no evidences of their development. C. The sediment surrounding the skeleton is permanently modified by the consequences of decay. The YBR sequence is dotted above the nodule because it was never observed in the field.

Figure captions

Fig. 1. Geographic and geomorphological settings of the Ica desert. A. Sketch map of Peru, with location of the Ica desert. B. Location of the sites of investigation, Cerro Colorado and Cerro Los Quesos. C. The landscape at Cerro Colorado, with a concretion hiding a vertebrate fossil skeleton standing in relief in the foreground. The hammer is circled in red for scale.

Fig. 2. Carbonatic nodules enclosing fossils, Pisco Fm. A. Skull and articulated mandibles of Cetotheriidae (Cetacea, Mysticeti, specimen CC-M22) (left); the skull, the mandibles and the postcranial skeleton (not visible in the photo) were hidden in a nodule, which was partially destroyed to reveal the bones. Bones are highlighted in yellow and the nodule in orange (right). B. Partially articulated skeleton including skull of Cetotheriidae CC-M18 (left); colors of bones and nodules (right) as in A. C. Complete articulated skeleton of small Cetotheriidae CC-M72 (left); colours of bones and nodule (right) as in A. D. Portion of rostrum of the holotype of the physeteroid *Livyatan melvillei* (Cetacea, Odontoceti, CC-O29) (left) and its position in the skull evidenced in light blue (right). Dolomite (orange) precipitated only around the teeth. E. Portion of articulated skeleton including skull of kentriodontid-like Delphinida (Cetacea, Odontoceti, CC-O4). Dolomite (orange) precipitated within the mesorostral groove, the endocranial, and the neural canals of the vertebrae. Although not visible in the figure, this specimens lies on a yellow sediment lying on a millimetric black Mn layer.

Fig. 3. Examples of fossils with partial or no concretions and of the enclosing sediment. A. Articulated skeleton of Balaenopteroidea (Cetacea, Mysticeti, CLQ-M58) with skull partially eroded. This specimen lies directly on the YBR sequence (see boxes). The lower dark grey layer is a volcanic ash bed (arrow). B. Portion of articulated vertebral column of Balaenopteroidea (CLQ- M33) lying on the YBR sequence. C. Disarticulated skeleton (skull, mandible, vertebrae and rib) of Cetotheriidae (Cetacea, Mysticeti, CC-M21) without nodule;

the diatomaceous sediment is reddened by some undetermined alteration process.

Fig. 4. Nodules distribution in the Cerro Colorado fossil vertebrate assemblage. A. Distribution of the nodules in the fossil vertebrate assemblage examined in this work at Cerro Colorado, as a function of the position along the stratigraphy. The represented stratigraphic interval is the Lower Allomember, where a higher concentration of fossils was found; red lines at the base and top of the section represent respectively the Pisco Fm.-Chilcatay Fm. angular unconformity and the Pisco Fm. intraformational angular unconformity (Di Celma et al., 2015). Elevations are in respect to the base of the section. Red ellipses along the stratigraphic column represent nodular dolomitic layers unrelated to the presence of vertebrate remains. Concentration of fossil specimens between 40 m and 75 m is due to the better exposure of the strata within that interval at Cerro Colorado (Bianucci et al., 2015). B. Presence of well-developed or partially developed concretions in the whole fossil assemblage (N=157) of Cerro Colorado. C, D, E. Nodules relationships with taxa, completeness and articulation.

Fig. 5. Sampling strategy. A. Sampling of concretions and bones in a mysticete skeleton (specimen CLQ-M1 shown as example). B. Schematic section of a bone enclosed in a dolomitic nodule. Red rectangles show the position of oriented subsamples. C. Example of the use of oriented subsamples: variation of extent of dolomite filling in an external nodule were studied. SEM-BSEI images and microanalytical informations from specimen CC-M22.

Fig. 6. SEM images and transmitted light microscope photographs of nodules thin sections. A. Dolomite infilling trabecular tissue of specimens CLQ-M1 (transmitted light, plane nicols); forams and diatoms (arrowheads) are visible within the aphanotopic dolomitic cement. B. Diatom within the nodule of specimen CC-M85 (SEM-BSE). The silica of the frustules was not dissolved (white star in the box) and dolomite completely filled the areolae (black star in the box). C. Examples of iron oxide framboid, formerly sulphide (left) and iron hydroxides filling a diatom frustule in the dolomite of specimen CC-M85 (right). D. Broken trabeculae rimmed by dolomite. E. Dolomite crystals nucleated on the trabeculae before the sediment

filled the voids of the trabecular tissue (specimen CLQ-M1) (SEM-BSE). Arrows point the boundary between the dolomite rim and the filling (and dolomitized) sediment F. A detail of iron oxides (arrowheads) associated to the dolomite rim seen in (E). G. An evident zoning in composition in the drusy dolomite is revealed by SEM-BSE images. H. Internal mould of diatom areolae made of Mn minerals (YBR of specimen CLQ-C67).

Fig. 7. Effect of dolomite precipitation on diagenetic compaction. Comparison between (A) *Coscinodiscus* frustules in a dolomitized mudstone from a nodule and (B) in the diatomaceous mudstone far from any dolomitc concretion. Early precipitated dolomite (A) prevented frustules from being squeezed by the sedimentary load (B). Arrows facing each other point to valves of the same frustule.

Fig. 8. Different types of microborings characterizing the cortical tissue of fossil whales from the Pisco Fm. A. Type A associated to Fe oxides (arrows; diameter of the framboid is ca. 7 μm). B. Microborings type B interesting the outer 50 μm of the cortical bone tissue of specimen CLQ-M10. C. Microborings type C characterize the cortical tissue of a vertebra of specimen CLQ-M67.

Fig. 9. Dolomite formation reconstruction. A. Marine vertebrate deposited at the sea floor. B. The consumption of the soft tissue is rapid (a few years, Treude et al., 2009) compared to lipid degradation. The skeleton was rapidly buried (see paragraph 5.1 for explanation). Rapid burial affected the skeleton. Sulphate reducing bacteria are represented: these could be closely related to the sulphate-reducing organisms of the whale-fall sulphophilic stage (lasting from 2 to 50 yrs, Smith and Baco 2003). The mobile scavenger stage and the enrichment opportunist stage are not represented because we found no evidences of their development. C. The sediment surrounding the skeleton is permanently modified by the consequences of decay. The YBR sequence is dotted above the nodule because it was never observed in the field.

Table
Click here to download Table: table 1.xlsx

site		specimen	identification	articulation	completeness	carbonate concretions	YBR	specimen short description	samples short description	type of analysis	figure
CERRO COLORADO	Mysticeti	CC-M85	Mysticeti indet.	n.d.	n.d.	complete outer nodule	visible	eroded skull and bone fragments	nodule and adjacent bone, YBR	petrography, SEM-EDS, XRPD	-
		CC-M22	Cetotheriidae indet.	high	medium	complete outer nodule	absent or covered	articulated skeleton including skull and mandibles inside a nodule	outer nodule and yellow layer	petrography, SEM-EDS	2A
	Odontoceti	CC-O29	*Livyatan melvillei*	low	low	partial	visible	skull, mandibles and teeth partially eroded	outer nodule, YBR	petrography	2D
		CC-O46	Odontoceti	high	low	partial outer nodule interesting vertebrae	absent	skull and few articulated vertebrae	nodule enclosing vertebrae	petrography, SEM-EDS	-
		CC-O4	aff. Kentriodontidae indet.	high	high	partial	visible	articulated skeleton including skull and mandibles	nodule in neural arc, mesorostral canal and endocranium, YBR	macroscopic observation	2E
		CC-O37	*Messapicetus gregarius*	medium	high	partial external nodule only on the articulated lumbar vertebrae.	visible	partially disarticulated skeleton (skull, mandibles, vertebrae, ribs, scapula, humeri and radius)	nodule in neural arc, intervertebral dolomite, external nodule on lumbar vertebrae, YBR	macroscopic observation	-
		CC-O35	*Messapicetus gregarius*	medium	medium	no outer nodule	-	partially disarticulated incomplete skeleton (skull, mandibles, cervical and thoracic vertebrae, ribs and sternum)	nodule partially filling endocranium	macroscopic observation	-
	Pinnipedia	CC-P7	Phocidae indet.	high	high	scarcely cemented nodule	-	articulated skeleton inside a small nodule	trabecular bone and sediment	SEM-EDS	-
CERRO LOS QUESOS	Mysticeti	CLQ-A1	Balaenopteroidea indet.	high	high	complete outer nodule	visible	complete skeleton including skull, mandibles and humerus	outer nodule, dolomite filling in trabecular bone of rib, YBR	petrography, SEM-EDS	-
		CLQ-A177	Mysticeti indet.	high	high	nearly complete outer nodule; only last vertebrae are not enclosed in a nodule	-	skull, mandibles, vertebral column	outer nodule, nodule in mesorostral canal, YBR	petrography, SEM-EDS	-
		CLQA-179	aff. Balaenopteroidea indet.	high	high	partial outer nodule interesting lumbar vertebrae	visible	nearly complete vertebral column	outer nodule of the lumbar vertebrae, intervertebral nodule, nodule filling mesorostral canal, YBR	petrography, SEM-EDS	-
		CLQ-A105	Balaenopteroidea indet.	low	low	no outer nodule	absent or covered	skull and articulated mandibles	nodule filling endocranium	petrography	-
		CLQ-A118	Mysticeti indet.	n.d.	low	no outer nodule	-	weathered skull	nodule filling endocranium	petrography	-
		CLQ-A125	Balaenopteroidea indet.	medium	high	no outer nodule	visible	partially articulated skeleton including skull, mandibles, vertebrae, ribs and humerus, without caudal portion	nodule filling endocranium, YBR	macroscopic observation	-
		CLQ-A121	Balaenopteroidea indet.	low	medium	specimen in a basin-scale lithified layer	visible	disarticulated skeleton including skull, mandibles and vertebrae	nodule ovelying the skull (bone visible at the base of the sample), nodule in neural arc, YBR	petrography, SEM-EDS	-
		CLQA180	Balaenopteroidea indet.	low/absent	-	specimen in a basin-scale lithified layer	visible	probably complete but disarticulated skeleton	discontinuous YBR at the base of the lithified layer	SEM-EDS, XRPD	-
		CLQA124	Balaenopteroidea indet.	high	high	no outer nodule, YBR envelope	visible	articulated skeleton including right humerus (skull eroded)	YBR, with yellow layer underlying the skeleton	SEM-EDS, XRPD	3A

Table 2 revised

Click here to download Table: Table 2_ REVISED.docx

	NODULES								DRUSY DOLOMITE	
Specimen	CC-A126				CC-M22				CLQ-A1	
distance from bone	5-10 µm		200-250 µm		100-150 µm		200-250 µm			
	mean [4]	σ	mean [3]	σ	mean [8]	σ	mean [8]	σ	core	rim
SiO_2 (wt%)	32,62	1,81	36,33	2,90	41,41	2,03	49,04	1,79	-	-
TiO_2	0,14	0,11	0,21	0,11	0,35	0,20	0,42	0,15	-	-
Al_2O_3	9,10	0,52	11,14	2,54	9,74	0,77	11,77	0,57	-	-
FeO	2,04	0,42	2,57	1,03	1,52	0,24	2,39	0,19	0,42	4,87
MnO	0,14	0,11	0,26	0,23	0,21	0,26	0,21	0,11	0,12	0,14
MgO	18,82	0,64	15,37	2,95	14,14	0,96	9,39	1,22	38,38	33,97
CaO	34,27	1,55	31,22	3,70	29,30	1,79	22,99	1,13	61,08	61,01
Na_2O	1,77	0,24	1,71	0,19	1,78	0,23	2,03	0,35	-	-
K_2O	1,05	0,15	1,19	0,09	1,35	0,06	1,72	0,26	-	-
P_2O_5	0,05	0,06	0,00	0,00	0,21	0,19	0,04	0,05	-	-
Sum	100,00		100,00		100,02		100,00		100,00	100,00

Figure 1
Click here to download high resolution image

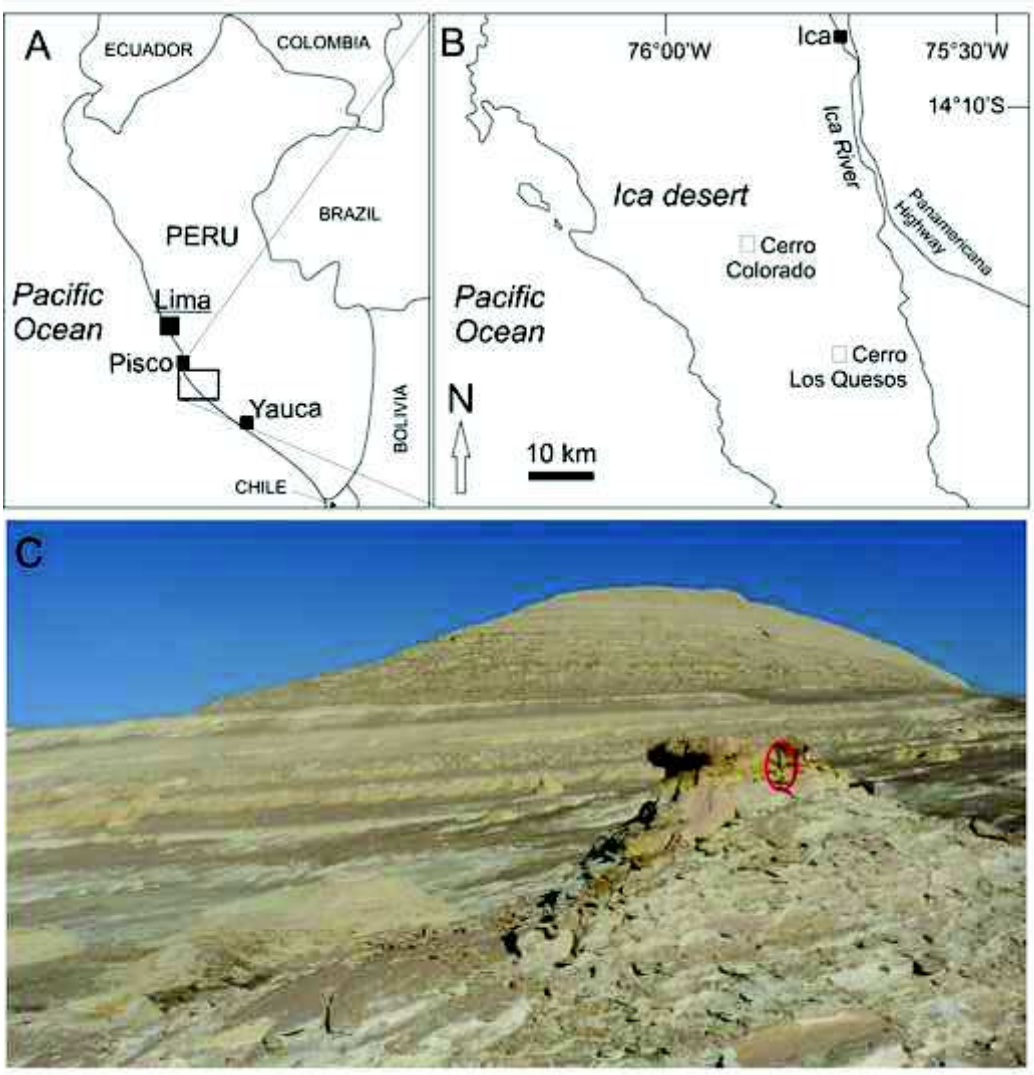

Figure 2 Revised
Click here to download high resolution image

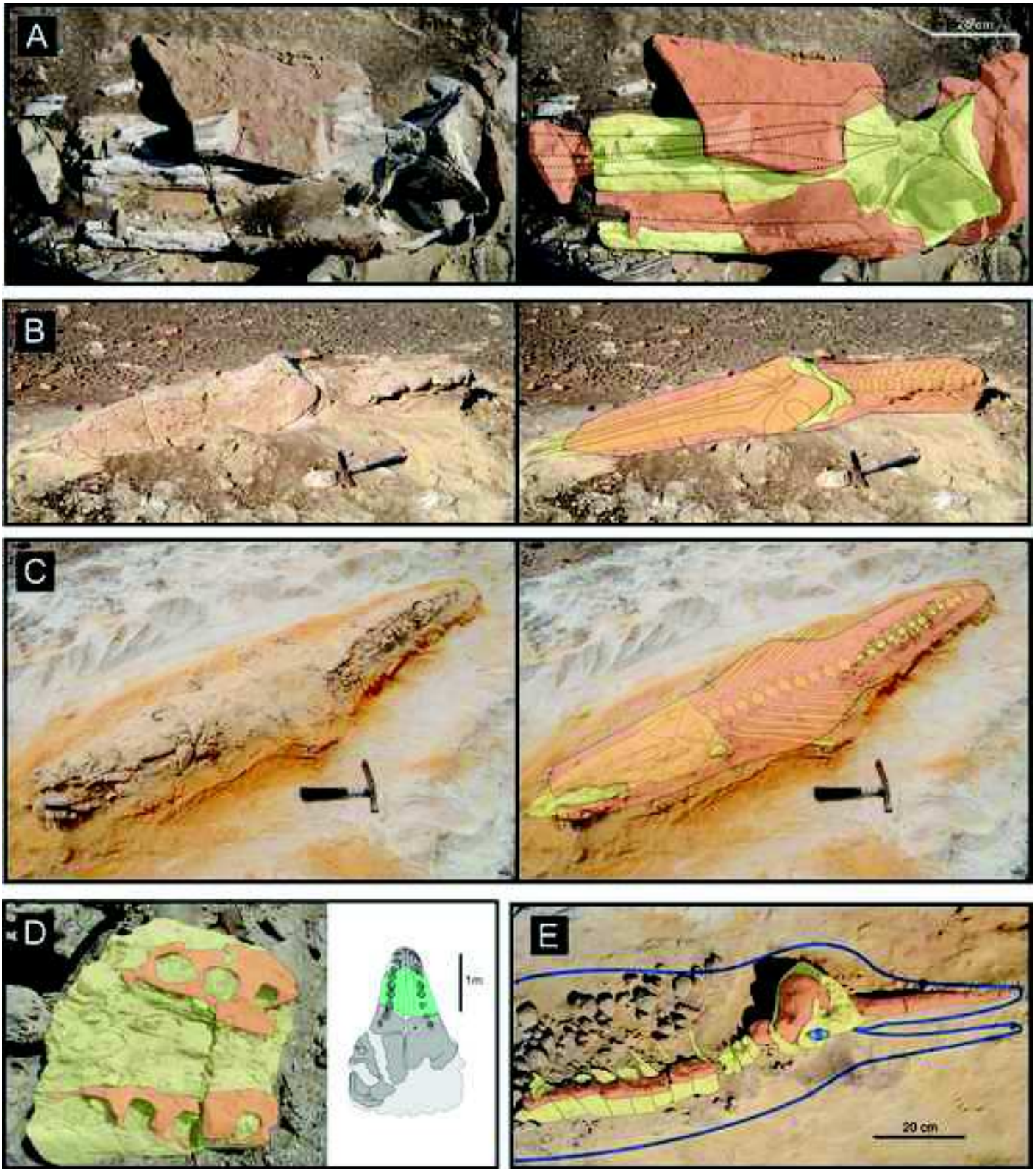

Figure 3 Revised
Click here to download high resolution image

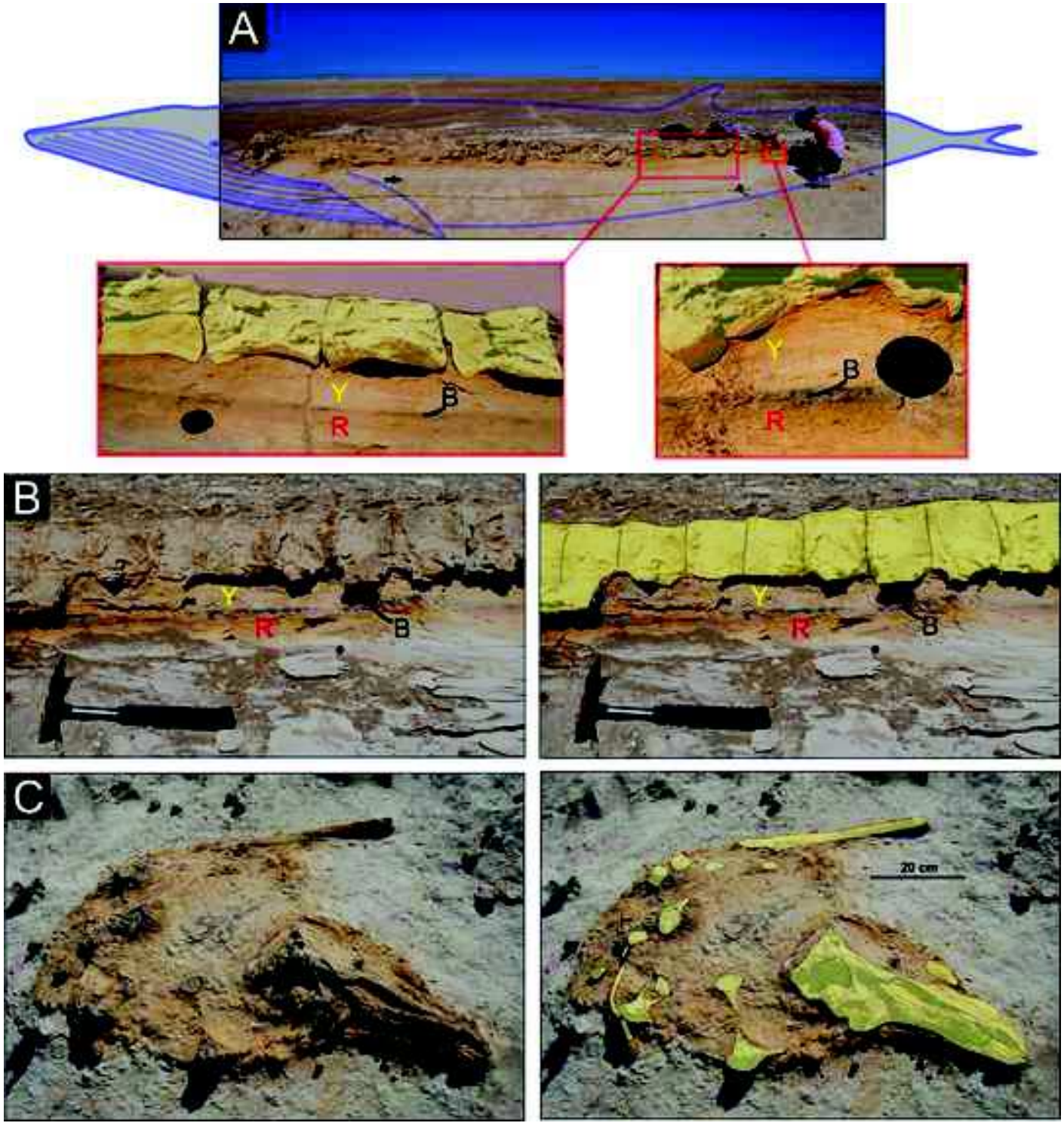

Figure 4 revised
Click here to download high resolution image

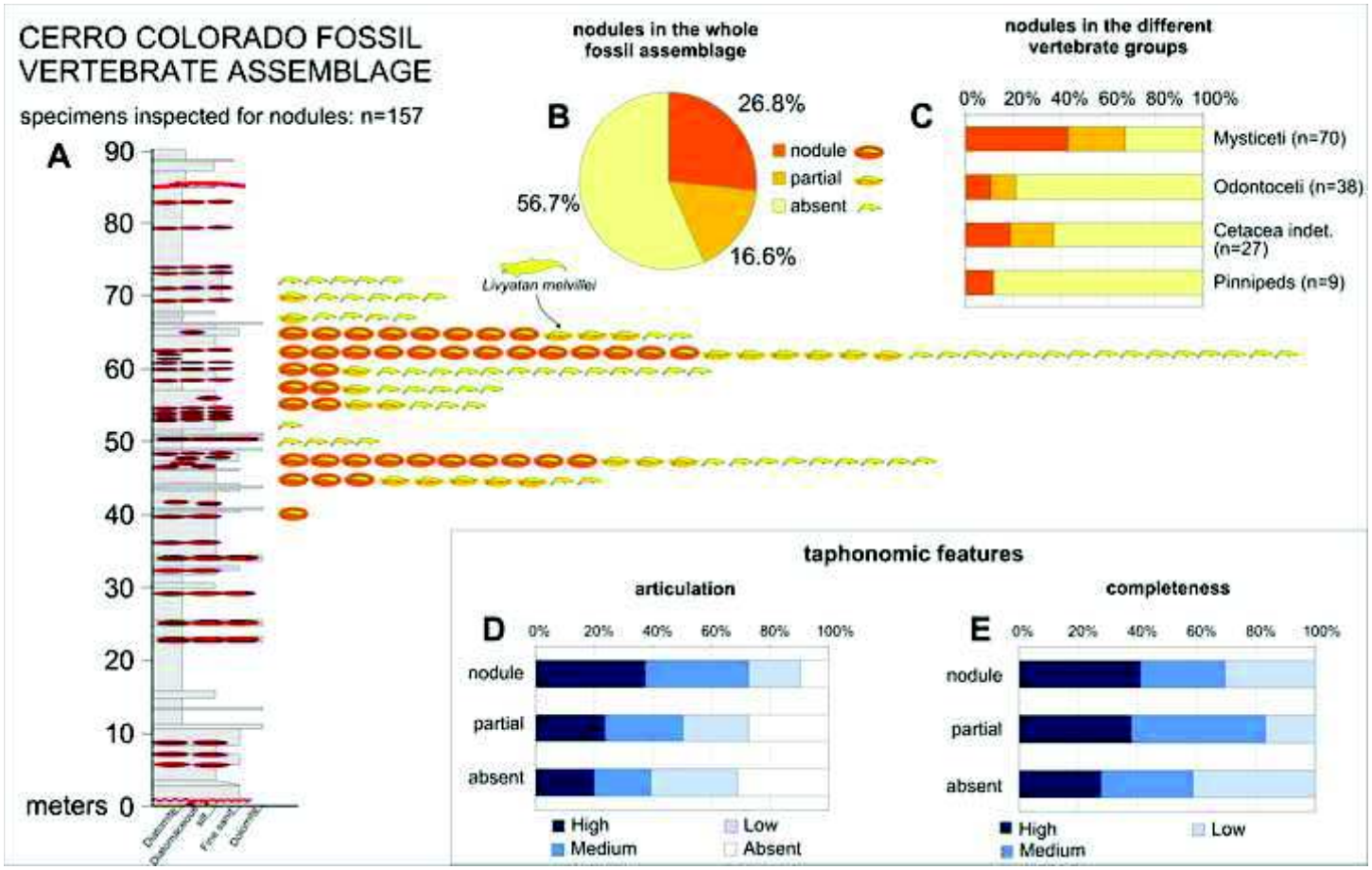

Figure 5 revised
Click here to download high resolution image

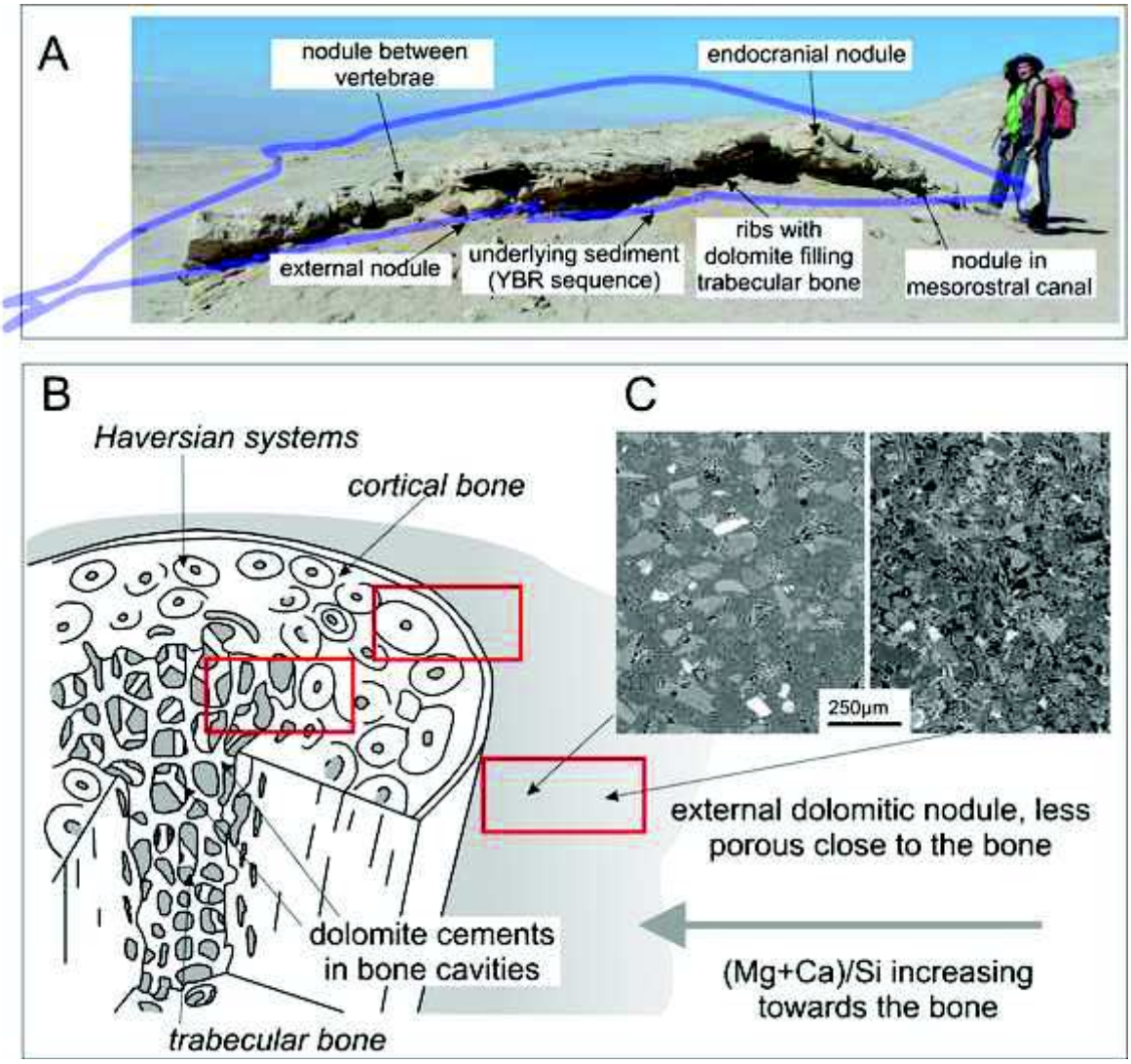

Figure 6 revised

Click here to download high resolution image

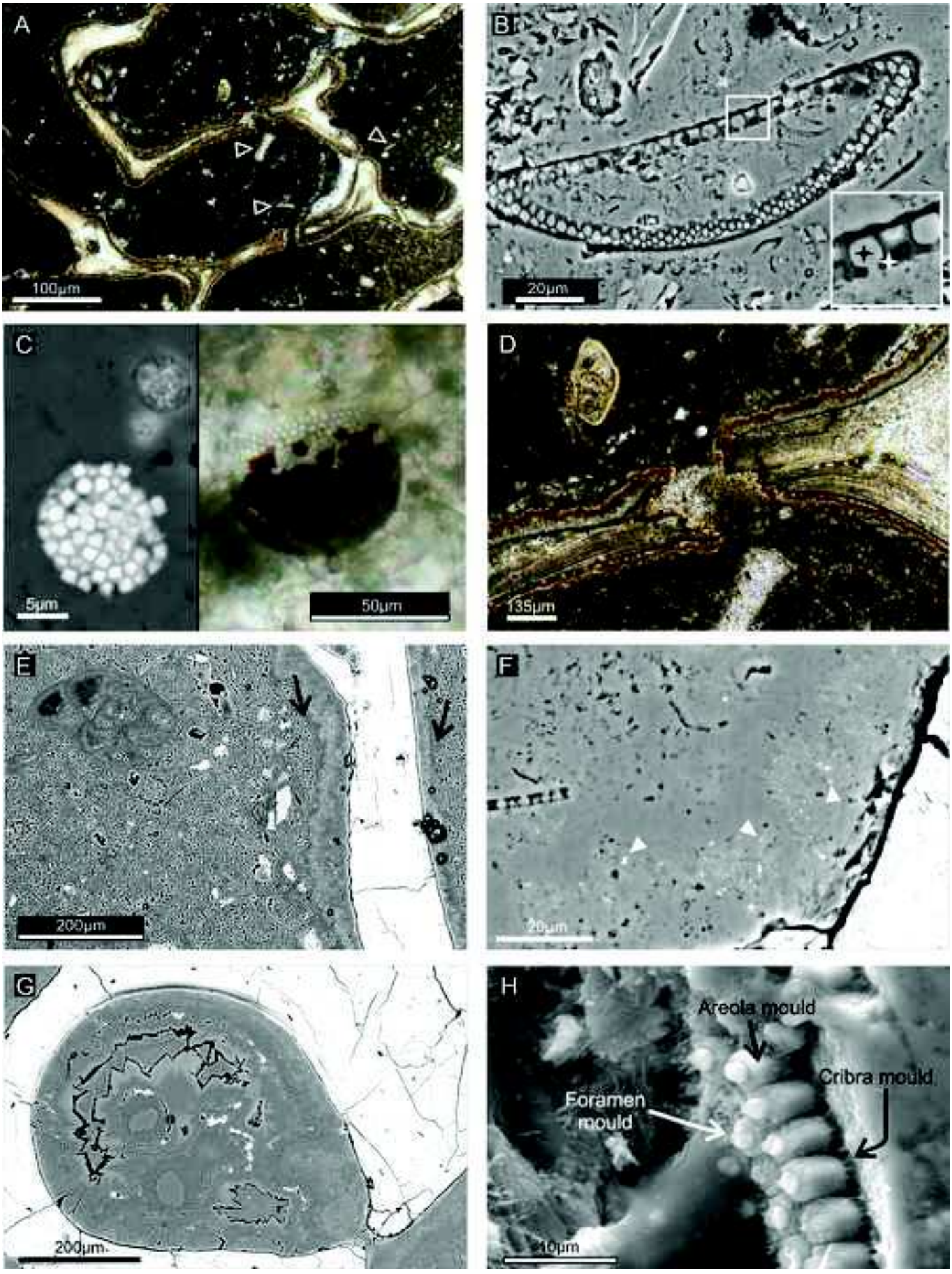

Figure 7 revised
Click here to download high resolution image

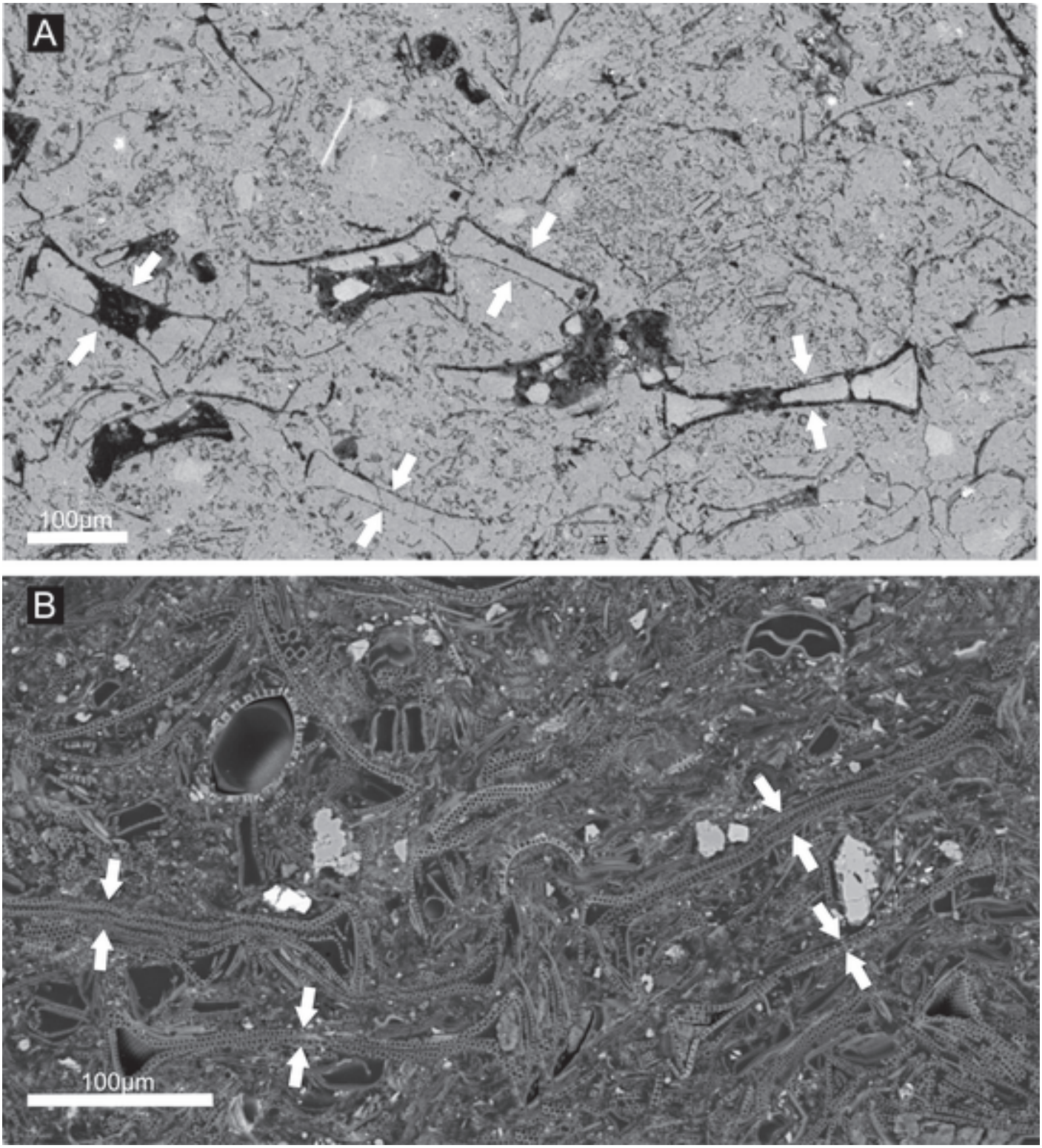

Figure 8 revised
Click here to download high resolution image

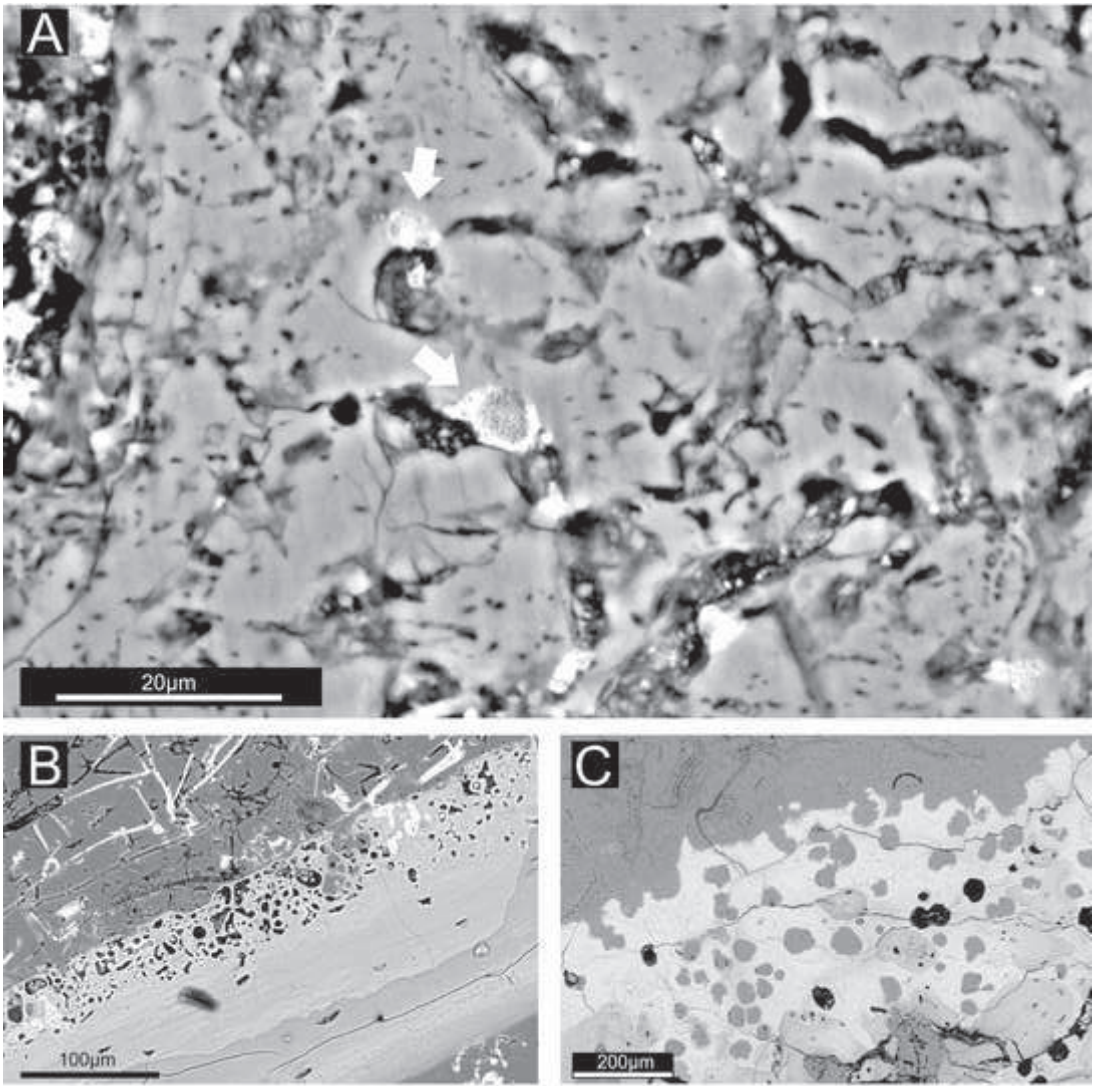

Figure 9 revised
Click here to download high resolution image

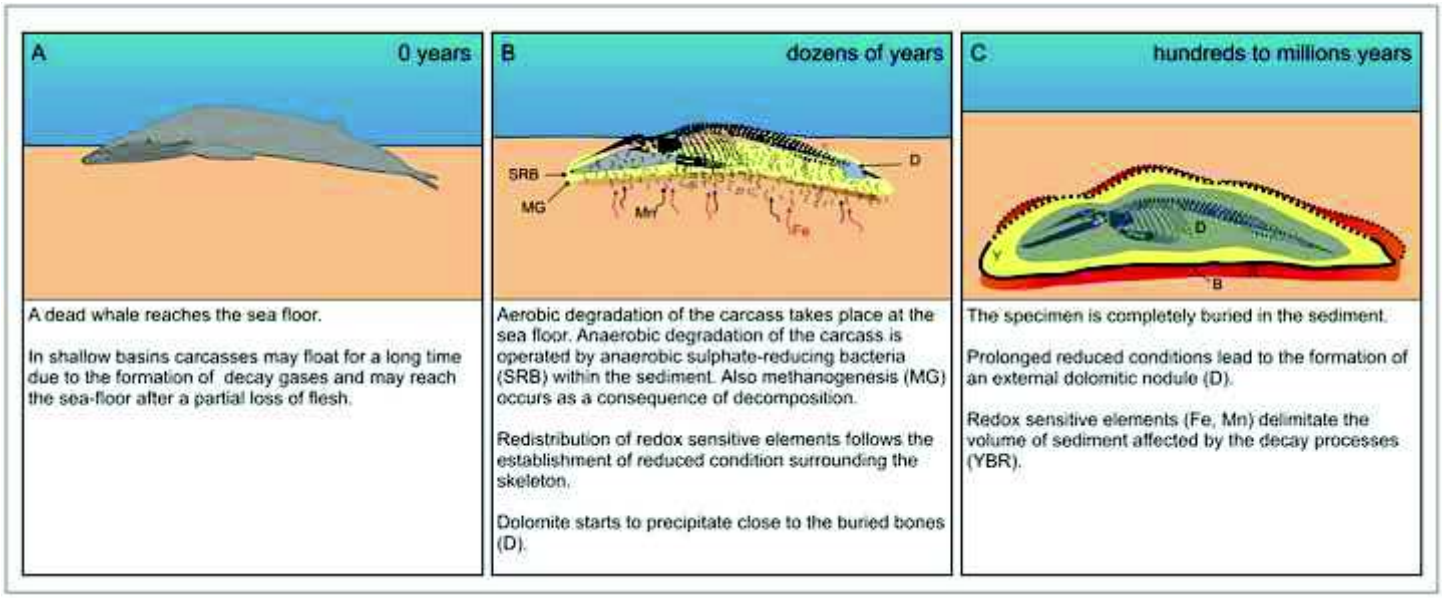

Supplementary material - table captions

Click here to download Background dataset for online publication only: Supplementary material_tables captions.docx

Supplementary material - figure captions

Click here to download Background dataset for online publication only: Supplementary material_figure captions.docx

Table S1

Click here to download Background dataset for online publication only: Supplementary material_Table_S1.xls

Table S2

Click here to download Background dataset for online publication only: Supplementary material_Table_S2.xls

Figure S1

Click here to download Background dataset for online publication only: Supplementary material_Figure S1.jpg

Figure S2

Click here to download Background dataset for online publication only: Supplementary material_Figure S2.jpg

Figure S3

Click here to download Background dataset for online publication only: Supplementary material_Figure S3.jpg

Supplementary material - references

Click here to download Background dataset for online publication only: References of Supplementary Material.docx